Homeostatic Synaptic Plasticity of Miniature Excitatory Postsynaptic Currents in Mouse Cortical Cultures Requires Neuronal Rab3A

Andrew G. Koesters[1*], Mark M. Rich[2], and Kathrin L. Engisch[3]

[1]Department of Pharmacology, Physiology, and Neurobiology, University of Cincinnati College of Medicine, Cincinnati, OH 45267, USA
[2]Department of Neuroscience, Cell Biology and Physiology, Boonshoft School of Medicine, Wright State University, Dayton, OH 45345
[3]Department of Neuroscience, Cell Biology and Physiology, Boonshoft School of Medicine and the College of Science and Mathematics, Wright State University, Dayton, OH 45435

*Andrew G. Koesters –Corresponding author
Department of Pharmacology, Physiology, and Neurobiology, University of Cincinnati College of Medicine, Cincinnati, OH 45267, USA
koesteag@ucmail.uc.edu, ph 513-558-2819

Author contributions: A.G.K., K.L.E. and M.M.R. designed research; A.G.K. performed research; A.G.K. and K.L.E. analyzed data; A.G.K, K.L.E., and M.M.R. wrote the paper.

ORCID iDs: ; A.G.K, https://orcid.org/0000-0003-3281-188X; M.M.R., https://orcid.org/0000-0002-6956-5531; K.L.E., https://orcid.org/0000-0002-1058-5343

The authors have no competing interests.

Keywords: Homeostatic Synaptic Plasticity; Synaptic Scaling; mEPSCs; Rab3A; AMPA receptors

Acknowledgements: The authors thank E. Whitlock and H. Ghouse for their contributions to confocal image analyses. This work was partially supported by NINDS P01 NS057228, Tim Cope, PI, KE, PI project 4.

30 Abstract

31 Following prolonged activity blockade, amplitudes of miniature excitatory postsynaptic currents
32 (mEPSCs) increase, a form of plasticity termed "homeostatic synaptic plasticity." We previously
33 showed that a presynaptic protein, the small GTPase Rab3A, is required for full expression of
34 the increase in miniature endplate current amplitudes following prolonged blockade of action
35 potential activity at the mouse neuromuscular junction in vivo (Wang et al., 2011), but it is
36 unknown whether this form of Rab3A-dependent homeostatic plasticity shares any
37 characteristics with central synapses. We show here that homeostatic synaptic plasticity of
38 mEPSCs is impaired in mouse cortical neuron cultures prepared from Rab3A$^{-/-}$ and mutant mice
39 expressing a single point mutation of Rab3A, Rab3A Earlybird mice. To determine if Rab3A is
40 involved in the well-established homeostatic increase in postsynaptic AMPA-type receptors
41 (AMPARs), we performed a series of experiments in which electrophysiological recordings of
42 mEPSCs and confocal imaging of synaptic AMPAR immunofluorescence were assessed within
43 the same cultures. We found that the increase in postsynaptic AMPAR levels was more variable
44 than that of mEPSC amplitudes, suggesting other factors may contribute to the homeostatic
45 increase in synaptic strength. Finally, we demonstrate that Rab3A is acting in neurons because
46 only selective loss of Rab3A in neurons, not glia, disrupted the homeostatic increase in mEPSC
47 amplitudes. This is the first demonstration that a protein thought to function presynaptically is
48 required for homeostatic synaptic plasticity of quantal size.

49

50

51 Introduction

52 One of the most studied phenomena triggered by prolonged activity blockade is the
53 increase in amplitudes of miniature excitatory postsynaptic currents (mEPSCs) in neurons. First
54 demonstrated in cultures of dissociated cortical neurons (Turrigiano et al., 1998) and spinal
55 cord neurons (O'Brien et al., 1998), the compensatory response to prolonged loss of activity has
56 been dubbed “homeostatic synaptic plasticity” (Turrigiano and Nelson, 2004; Pozo and Goda,
57 2010). These first two studies provided evidence that glutamate receptors were also increased
58 after prolonged inactivity, via an increased response to exogenously applied glutamate
59 (Turrigiano et al., 1998) and increased immunofluorescent labeling of GluA1 receptors at
60 synaptic sites (O'Brien et al., 1998). The accompanying increase in synaptic AMPA receptors has
61 been confirmed with immunofluorescence in multiple studies of hippocampal and cortical
62 cultures treated with TTX, including (Wierenga et al., 2005; Hou et al., 2008; Ibata et al., 2008;
63 Jakawich et al., 2010; Tatavarty et al., 2013; Xu and Pozzo-Miller, 2017; Dubes et al., 2022). It is
64 now well accepted that the homeostatic increase in mEPSC amplitudes in neurons is due to an
65 increase in postsynaptic AMPA receptors.

66 In our previous work, we found that a TTX cuff applied for 48 hrs around the sciatic
67 nerve in mice led to an increase in the amplitude of the miniature endplate currents (mEPCs)
68 recorded in tibialis anterior muscles. Surprisingly, and unlike at central synapses, we could find
69 no evidence that the acetylcholine receptors levels at the neuromuscular junction (NMJ) were
70 increased in the TTX-cuff treated mice (Wang et al., 2005). This result led us to search for
71 presynaptic molecules that might homeostatically regulate the presynaptic quantum. In
72 previous studies in chromaffin cells, we identified the small GTPase Rab3A, a presynaptic vesicle

73 protein, as a regulator of synaptic vesicle fusion pore opening (Wang et al., 2008), so we
74 examined whether deletion of Rab3A (Rab3A$^{-/-}$) might prevent homeostatic upregulation of
75 mEPC amplitude at the NMJ. The results were clear: the homeostatic increase in mEPC
76 amplitude induced by the TTX cuff was strongly reduced in the Rab3A$^{-/-}$ mouse, and was
77 completely abolished in the Earlybird mutant (Rab3A$^{Ebd/Ebd}$), which has a single point mutation
78 in Rab3A that causes a shift towards early awakening due to a shorter circadian period, that is
79 more dramatic than that of the Rab3A deletion mouse (Kapfhamer et al., 2002; Wang et al.,
80 2011). These results led us to conclude that the homeostatic increase in mEPC amplitude at the
81 NMJ is a presynaptic phenomenon.

82 It has remained somewhat of a mystery what the role of Rab3A is in synaptic
83 transmission. The Rab3A$^{-/-}$ mouse has minimal phenotypic abnormalities, with evoked synaptic
84 transmission and mEPSCs essentially normal in hippocampal slices (Geppert et al., 1994). At the
85 Rab3A$^{-/-}$ NMJ, reductions in evoked transmission were detected, but only under conditions of
86 reduced extracellular calcium (Coleman et al., 2007). There are some modest changes in short
87 term plasticity during repetitive stimulus trains, with increased depression observed in
88 response to moderate frequencies in hippocampal slices (Geppert et al., 1994) and at the
89 mammalian NMJ (Coleman and Bykhovskaia, 2009), but increased facilitation in response to
90 high frequency stimulation at the mammalian NMJ (Coleman and Bykhovskaia, 2010). The most
91 dramatic effect of loss of Rab3A is the abolishment of a presynaptic form of long-term
92 potentiation (LTP) at the mossy fiber-CA3 synapse that is induced by 25 Hz stimulation in the
93 presence of NMDA blockers (Weisskopf et al., 1994; Castillo et al., 1997). Our result that
94 prolonged inactivity-induced plasticity of mEPC amplitude at the mammalian NMJ is disrupted

95 with loss of function of Rab3A further cements a role for Rab3A in activity-dependent plasticity
96 of synaptic strength. However, a crucial question that remains is whether the TTX-cuff induced
97 effect on the amplitude of the spontaneous synaptic current at the NMJ shares underlying
98 mechanisms with central synapses. We set out to answer this question for the more well-
99 studied phenomenon of homeostatic plasticity of mEPSCs in dissociated mouse cortical neurons
100 prepared from wild type, Rab3A$^{-/-}$ mice and Rab3a$^{Ebd/Ebd}$ mice treated with TTX for 48 hrs. We
101 show here that homeostatic synaptic plasticity of mEPSC amplitude was strongly reduced in
102 cultures from Rab3A$^{-/-}$ mice, and completely abolished in cultures from Rab3A$^{Ebd/Ebd}$ mice,
103 supporting a shared mechanism with the neuromuscular junction.

104

105

106 Results

107 We previously reported that mixed cultures of cortical neurons and glia prepared from
108 postnatal day 0-2 mouse pups responded to a block of action potential-mediated activity by a
109 48 hr TTX treatment with an increase in mEPSC amplitude (Hanes et al., 2020). Here, we asked
110 the question whether cortical cultures prepared from mice lacking the small GTPase Rab3A, or,
111 expressing a point mutation of Rab3A, Rab3A Earlybird, have an altered homeostatic plasticity
112 response to a prolonged loss of network activity. The Rab3A Earlybird mutation was discovered
113 in a mutagenesis screen in mice for genes involved in the rest-activity cycle (Kapfhamer et al.,
114 2002). In that study, the authors concluded that the Earlybird mutation was likely dominant-
115 negative, as the shift in circadian period was substantially more dramatic than that observed in
116 the Rab3A$^{-/-}$ mice. As described in the Introduction, the effects of loss of Rab3A have been
117 modest, so we included experiments using the Rab3A Earlybird mutant mice to see if there
118 would be a more robust phenotype, and in doing so, strengthen our conclusions based on the
119 Rab3A deletion mice. To obtain Rab3A$^{-/-}$ and Rab3A$^{Ebd/Ebd}$ homozygotes, we established two
120 mouse colonies of heterozygous breeders with cultures prepared from pups derived from a
121 final breeding pair of homozygotes. Although we backcrossed Rab3A$^{+/-}$ with Rab3A$^{+/Ebd}$ for 11
122 generations, clear differences in mEPSC amplitudes in untreated cultures (see below) and in
123 calcium current amplitudes in adrenal chromaffin cells (unpublished obs.) remained. Therefore,
124 throughout this study we keep the two strains separate and there are two Rab3A$^{+/+}$ or 'wild
125 type' phenotypes.

126 We found that loss of Rab3A resulted in a greatly impaired homeostatic increase after
127 activity blockade. Example current traces of spontaneously occurring mEPSCs recorded from

128 pyramidal neurons in untreated (CON) 13-14 DIV cortical cultures and sister cultures treated
129 with 500 nM TTX for 48 hr prepared from wild type and Rab3A$^{-/-}$ mice in the Rab3A$^{+/-}$ colony are
130 shown in Figures 1A and B, respectively. Average mEPSC waveforms from the same recordings
131 are shown in Figures 1C and D. The mean mEPSC amplitudes for 30 control and 23 TTX-treated
132 neurons from Rab3A$^{+/+}$ cultures are displayed in the box and whisker plot in Figure 1E; after
133 activity blockade the average mEPSC amplitude increased from 13.9 ± 0.7 pA to 18.2 ± 0.9 pA.
134 In contrast, in cultures prepared from Rab3A$^{-/-}$ mice, the average mEPSC amplitude was not
135 significantly increased, for 25 untreated cells and 26 TTX-treated cells (Figure 1F, 13.6 ± 0.1 pA
136 vs. 14.3 ± 0.6 pA). We found that TTX treatment also resulted in an increase in mEPSC
137 frequency in cultures prepared from Rab3A$^{+/+}$ mice, as shown in Figure 1G (CON, 2.26 ± 0.37
138 sec^{-1}; TTX, 4.62 ± 0.74 sec^{-1}). This TTX-induced frequency increase was strongly reduced in
139 cultures from Rab3A$^{-/-}$ mice, but there were a few outliers with very high frequencies still
140 present after TTX treatment (Figure 1H, CON, 2.74 ± 0.49 Hz; TTX, 3.23 ± 0.93 Hz).
141 We next examined homeostatic plasticity in cultures prepared from wild type mice in
142 the Rab3A$^{+/Ebd}$ colony. Example current traces of mEPSCs, and average mEPSC waveforms, are
143 shown in Figures 2A and C, respectively, for cortical cultures prepared from wild type mice in
144 the Rab3A$^{+/Ebd}$ colony. Treatment with TTX for 48 hr led to a significant increase in the average
145 mEPSC amplitude of 23 TTX-treated cells when compared to 20 untreated cells (Figure 2E, CON,
146 11.0 ± 0.6 pA; TTX, 15.0 ± 1.3 pA). We note here that while the two wild type strains respond
147 very similarly to activity blockade, the mean mEPSC amplitude in untreated cultures was
148 significantly different in the two wild type strains, 13.9 ± 0.7 pA, wild type from Rab3A$^{+/-}$ colony;
149 11.0 ± 0.6 pA, wild type from Rab3A$^{+/Ebd}$ colony ($p = 0.004$, Kruskal-Wallis test).

150 We found a complete disruption of homeostatic plasticity in cortical cultures prepared
151 from Rab3A$^{Ebd/Ebd}$ mice, as can been seen in viewing example mEPSC traces and average mEPSC
152 waveforms (Figures 2B and D, respectively). The lack of TTX effect was confirmed in a
153 comparison of mEPSC amplitude means for 21 untreated and 22 TTX-treated cells (Figure 2F,
154 CON, 15.1 ± 1.0 pA vs. TTX, 14.6 ± 1.1 pA). There was a trend towards increased mEPSC
155 frequency in TTX-treated cultures from this wild type strain, but the difference was not as
156 robust as for the wild type cultures from Rab3A$^{+/-}$ colony, and did not reach statistical
157 significance (Figure 2G, CON, 1.15 ± 0.19 sec^{-1}; TTX, 2.54 ± 0.55 sec^{-1}). This trend was not
158 observed in neurons from cultures prepared from Rab3A$^{Ebd/Ebd}$ mice, likely due to an increase in
159 frequency in untreated cells—frequencies remained high in TTX-treated cells (Figure 2H, CON,
160 1.71 ± 0.41 sec^{-1}; TTX, 3.05 ± 0.80 sec^{-1}). Our results show that the homeostatic increase in
161 mEPSC amplitude after activity blockade is disrupted in both Rab3A$^{-/-}$ and the Rab3A$^{Ebd/Ebd}$
162 cortical neurons, strongly supporting a crucial role of functioning Rab3A in this process.
163 The disruption in homeostatic plasticity differs for Rab3A$^{-/-}$ and Rab3A$^{Ebd/Ebd}$. In the
164 Rab3A$^{-/-}$ data set, mEPSCs from untreated cultures were indistinguishable from mEPSCs from
165 Rab3A$^{+/+}$ untreated cultures, demonstrating loss of Rab3A has no impact on basal activity
166 mEPSC amplitudes. In the Rab3A$^{Ebd/Ebd}$ data set, mEPSC amplitudes from untreated cultures
167 were significantly larger than those of untreated cultures from wild type mice, as can be seen
168 comparing the CON values in Figures 2E and F (CON, Rab3A$^{+/+}$, 11.0 ± 0.7 pA, vs. CON,
169 Rab3A$^{Ebd/Ebd}$, 15.1 ± 1.0 pA, $p = 0.0027$, Kruskal-Wallis test). The increase in mEPSC amplitude in
170 cultures from Rab3A$^{Ebd/Ebd}$ mice is consistent with the increase in mEPC amplitude we observed
171 at the Rab3A$^{Ebd/Ebd}$ NMJ (Wang et al., 2011).

The small GTPase Rab3A is generally thought to function presynaptically to regulate synaptic vesicle trafficking, possibly in an activity-dependent manner (Castillo et al., 1997; Lonart et al., 1998; Leenders et al., 2001; Schluter et al., 2006; Coleman and Bykhovskaia, 2009; Tian et al., 2012). In contrast, homeostatic plasticity of mEPSC amplitude has been attributed to an increase in postsynaptic receptors on the surface of the dendrite (O'Brien et al., 1998; Turrigiano et al., 1998). At the NMJ in vivo, we could find no evidence for an increase in AChRs after TTX block of the sciatic nerve in vivo (Wang et al., 2005). Is Rab3A required for the homeostatic increase in surface AMPA-type glutamate receptors that has been confirmed by multiple studies (see Introduction)?

We explored whether Rab3A might be acting to increase postsynaptic AMPA receptors. In some studies of homeostatic synaptic plasticity it has been found that application of a Ca^{2+}-permeable AMPA receptor-specific inhibitor reversed the homeostatic increase in mEPSC amplitude (Ju et al., 2004; Thiagarajan et al., 2005; Sutton et al., 2006). Figure 3A shows that the *TTX-induced increase* in mean mEPSC amplitude was nearly identical in a set of 11 CON and 11 TTX-treated cells before and after treatment with 1-Naphthyl acetyl spermine trihydrochloride (NASPM), a synthetic analogue of the Ca^{2+}-permeable AMPA receptor inhibitor philanthotoxin (before NASPM, CON 12.9 ± 3.5 pA; TTX, 17.5 ± 3.1 pA; after NASPM, CON 11.9 ± 2.6 pA; TTX 16.1 ± 3.5 pA). This result indicates that the TTX-induced increase in mEPSC amplitude does not depend on Ca^{2+}-permeable receptors, since the effect of TTX clearly remained when their presence was removed by acute NASPM application. We do not think that there was any technical issue with the NASPM application, because overall, mEPSC amplitudes were reduced modestly in both untreated and TTX-treated cultures (Figure 3B, CON, before NASPM, 12.9 ±

194 3.5 pA; after NASPM, 11.9 ± 2.6 pA; TTX, before NASPM, 17.5 ± 3.1 pA; after NASPM, 16.1 ± 3.5
195 pA). Furthermore, NASPM consistently reduced mEPSC frequency (Figure 3C, CON, before
196 NASPM, 1.84 $\pm$ 0.55 sec^{-1}; after NASPM, 1.56 $\pm$ 0.53 sec^{-1}; TTX, before NASPM, 4.40 ± 3.51 sec^{-1};
197 after NASPM, 2.68 ± 2.25 sec^{-1}). Similar to the data in Figure 1, frequency is significantly
198 increased after TTX treatment ($p = 0.04$), but this difference is no longer significant after
199 NASPM application ($p = 0.20$). One explanation for the effect on frequency is that there are
200 synaptic sites that express only homomers of Ca^{2+}-permeable AMPA receptors (GluA2-lacking
201 AMPARs); mEPSCs from these sites would be expected to be completely blocked by NASPM
202 (see cartoon description in Figure 3D, Left). We cannot rule out an alternative explanation, that
203 presynaptic Ca^{2+}-permeable AMPA receptors normally enhance release probability, and NAPSM
204 prevents this action. The magnitude of the frequency reduction following acute NASPM appears
205 to be greater after TTX treatment, suggesting that loss of activity could promote the
206 establishment of synaptic sites that contain only Ca^{2+}-permeable receptors. However, these
207 new sites do not appear to contribute to the increase in mEPSC amplitude (Figure 3A). The lack
208 of effect of NASPM rules out the contribution of Ca^{2+}-permeable AMPA receptors GluA1, GluA3
209 and GluA4 (Hollmann et al., 1991; Burnashev et al., 1992; Jonas and Burnashev, 1995), as well
210 as Ca^{2+}-permeable forms of Kainate receptors GluA5 and GluA6 (Koike et al., 1997; Sun et al.,
211 2009) to homeostatic synaptic plasticity.

212 Having established that homomeric Ca^{2+}-permeable receptors are not contributing to
213 the homeostatic increase in mEPSC amplitude, we turned to immunofluorescence and confocal
214 imaging to assess whether GluA2 receptor expression, which will identify GluA2 homomers and
215 GluA2 heteromers, was increased in our wild type mouse cortical cultures following 48 hr

216 treatment with TTX. Since mEPSCs necessarily report synaptic levels of receptors, we used
217 VGLUT1-immunofluorescence to identify synapses on pyramidal primary apical dendrites
218 labeled with MAP-2 immunofluorescence. We focused on the primary dendrite of pyramidal
219 neurons as a way to reduce variability that might arise from being at widely ranging distances
220 from the cell body, or, from inadvertently sampling dendritic regions arising from inhibitory
221 neurons. In addition, it has been shown that the increase in receptors is most dramatic in this
222 region (Turrigiano et al., 1998). Figure 4 (Top) shows two pyramidal neurons, one from an
223 untreated culture on the left, and one from a TTX-treated culture on the right, prepared from
224 Rab3A$^{+/+}$ mice. To measure characteristics of synaptically located GluA2 receptor clusters, we
225 zoomed in on the primary dendrite (region in white rectangle). The zoomed regions for single
226 confocal sections of the selected area are shown below and contain pairs of VGLUT1- and
227 GluA2-immunofluorescent clusters indicated by white trapezoidal frames. A dendrite typically
228 required ~10 confocal sections to be fully captured, and the total number of synaptic pairs for
229 all the sections imaged on a dendrite averaged 20 (20.4 $\pm$ 6.5 (SD); range, 11-38) so this is an
230 atypically high number of pairs within a single section; these particular dendrites and sections
231 were selected for illustration purposes. In addition to the synaptic pairs, we observed many
232 GluA2-immunofluorescent clusters not associated with VGLUT1 immunofluorescence (a few are
233 indicated with white arrows), most probably extrasynaptic receptors. There were also GluA2-
234 positive clusters present outside of MAP2-positive dendrites, which may be located on
235 astrocytes (Fan et al., 1999). Finally, GluA2 immunofluorescent clusters close to VGLUT1
236 immunofluorescence but not located along any apparent MAP2-positive neurites suggests the
237 presence of axon-axonal contacts, although VGLUT1 has also been detected in astrocytes

238 (Ormel et al., 2012). Only sites that contained both VGLUT1 and GluA2 immunofluorescence
239 close to the primary MAP2-postive dendrite or a secondary branch along this primary dendrite
240 were selected for analyses. In the experiment from which these images were collected, we
241 analyzed the distance from the cell body for each synapse. The average distance from the cell
242 body, for dendrites from the untreated cell, was 38.5 $\pm$ 2.8 μm; for the TTX-treated cell, it was
243 42.4 $\pm$ 3.2 μm (p = 0.35, Kruskal-Wallis test). Since the greatest distance from the cell body is
244 set by the outer limit of the zoom window, and that window was placed adjacent to the cell
245 body, distances in other experiments would be in this same range.
246 Variability in the magnitude of the homeostatic response from culture to culture is
247 averaged out in physiological experiments by the pooling of data from many cells across many
248 cultures. To reduce the necessity for many cultures, we chose to pair experiments in the same
249 cultures by recording mEPSCs from one set of coverslips, and processing another set of
250 coverslips from the same culture for immunofluorescence. We also wanted to determine if the
251 homeostatic response of mEPSC amplitudes varied from culture to culture, and if so, whether
252 the GluA2 receptor levels varied in parallel. We completed this matched paradigm of physiology
253 and immunofluorescence-for 3 cultures prepared from Rab3A$^{+/+}$ mice. We first present the
254 results as means for each culture, for control and TTX-treated dishes, for mEPSC data (Figure
255 5A) and imaging data (Figure 5B). Levels of GluA2 immunofluorescence at synaptic sites were
256 quantified by the size of the GluA2-immunofluorescent receptor cluster, because this showed
257 the greatest response to activity blockade; the average intensity value, and the integral of
258 intensity values across the area of the cluster, are included in a summary of the data in Table 1.
259 Three of three cortical cultures showed an increase in mean mEPSC amplitude after TTX

260 treatment. In contrast, one of the same three cultures showed a decrease in mean GluA2
261 receptor cluster size. Therefore, the decrease in receptor levels in Culture #3 was due to
262 something other than a lack of homeostatic effect on mEPSCs in that culture. Because there
263 was a clear trend towards increased GluA2 receptor cluster size, but the receptor response
264 appears more variable, we performed immunofluorescence measurements on two additional
265 cortical cultures, both of which showed modest increases after TTX treatment (Figure 5C). We
266 confirmed that there was not an increase in GluA1 receptor levels in two matched cultures that
267 showed robust homeostatic increases in mEPSC amplitudes (Supplementary Figure 1A, culture
268 mean mEPSC amplitudes; Supplementary Figure 1B, culture mean GluA1 receptor cluster sizes).

269 We next pooled data from the multiple cultures to examine effects of activity blockade
270 on GluA2 receptors at the level of cell means. Because the average number of synaptic sites
271 identified in the primary dendrites in three cultures was 20.4, we also took 20 mEPSC samples
272 from each cell, the 21st to the 40th mEPSC recorded, to minimize any differences in variability
273 between GluA2 receptors and mEPSCs that might be due to a difference in sampling. In the
274 data pooled from the 3 matched experiments, neurons from Rab3A$^{+/+}$ cultures showed a
275 significant increase in mean mEPSC amplitudes following activity blockade (Figure 5D; Table 1).
276 This result indicates that the homeostatic response averaged across the 3 cultures was very
277 similar to, but slightly smaller than, that of the data set presented in Figure 1. The mean for size
278 of GluA2 immunofluorescent receptor clusters showed a trend towards higher values after
279 activity blockade (18.1%) that was of similar magnitude to the mEPSC amplitude increase
280 (19.7%), but did not reach statistical significance for 3 cultures (Figure 5E) or 5 cultures (Figure
281 5F; Table 1). As expected, mean mEPSC amplitude was not increased following activity

282 blockade in the data pooled from a new set of 3 Rab3A$^{-/-}$ cultures (Table 1). For
283 immunofluorescence results from the same Rab3A$^{-/-}$ cultures, no trend towards higher values
284 was apparent for GluA2 receptor cluster characteristics (Table 1). However, given the variability
285 of the GluA2 response in cultures from Rab3A$^{+/+}$ mice, it would require a much higher number
286 of Rab3A$^{+/+}$ and Rab3A$^{-/-}$ cultures to make any firm conclusions about the role of Rab3A in the
287 homeostatic response of GluA2 receptors.

288 Having used VGLUT1 immunofluorescence to mark synaptic sites, we could also ask
289 whether there was a presynaptic effect of activity blockade on the size, intensity or integral of
290 the VGLUT1 signal at sites apposed to the previously examined GluA2 postsynaptic sites. In the
291 pooled data from cultures prepared from Rab3A$^{+/+}$ mice, we found no change in the size of the
292 VGLUT1-positive regions, and trends towards reduced intensity and integral (Table 2). These
293 data do not support the idea that activity blockade caused an increase in the amount of
294 VGLUT1 per vesicle, although we cannot rule out that a simultaneous reduction in the number
295 of vesicles obscured the effect, since we did not have an independent label for synaptic
296 vesicles. In cultures prepared from Rab3A$^{-/-}$ mice, the size, intensity and integral of the VGLUT1-
297 positive regions did not significantly change (Table 2).

298 We have demonstrated here for the first time that the synaptic vesicle protein Rab3A
299 influences the homeostatic regulation of quantal amplitude. What are possible ways that
300 Rab3A could exert its effect? It has previously been shown that exogenous addition of TNFα to
301 hippocampal cultures causes an increase in surface expression of GluA1 receptors (although not
302 GluA2 receptors), and that the homeostatic increase in mEPSC amplitudes is abolished in
303 cultures prepared from the TNFα deletion mouse (Stellwagen et al., 2005; Stellwagen and

304 Malenka, 2006). Furthermore, neurons from TNF$\alpha^{+/+}$ mice plated on glial feeder layers derived
305 from TNF$\alpha^{-/-}$ mice fail to show the increase in mEPSC amplitude after TTX treatment, indicating
306 that the TNFα inducing the receptor increases following activity blockade comes from the glial
307 cells (Stellwagen and Malenka, 2006). It has recently been shown that the source of TNFα is
308 astrocytes rather than microglia (Heir et al., 2024). Rab3A has been detected in astrocytes
309 (Maienschein et al., 1999; Hong et al., 2016), so to determine whether Rab3A is acting via
310 regulating TNFα release from astrocytes, we performed experiments similar to those of
311 Stellwagen and Malenka (2006) (schema illustrated in Figure 6, Left). Under our culturing
312 conditions, the glial feeder layers would be expected to be composed mainly of astrocytes (Heir
313 et al., 2024). We compared the effect of activity blockade on mEPSC amplitudes recorded from
314 cortical neurons from Rab3A$^{+/+}$ mice plated on Rab3A$^{+/+}$ glial feeder layers (Figure 6A); neurons
315 from Rab3A$^{+/+}$ mice plated on Rab3A$^{-/-}$ glia (Figure 6B), and neurons from Rab3A$^{-/-}$ mice plated
316 on Rab3A$^{+/+}$ glia (Figure 6C). If Rab3A is required for TNFα release from glia, then Rab3A$^{+/+}$
317 neurons plated on Rab3A$^{-/-}$ glia should not show a homeostatic increase in mEPSC amplitude
318 after treatment with TTX, and any cultures with Rab3A$^{+/+}$ glia should have a normal homeostatic
319 response. We found the opposite result: mEPSC amplitudes increased dramatically in cultures
320 where Rab3A was present in neurons (WT on WT, CON, 13.3 $\pm$ 0.5 pA, TTX, 16.7 $\pm$ 1.2 pA; WT
321 on KO, CON, 13.3 $\pm$ 1.0 pA, TTX, 18.8 $\pm$ 1.4 pA), but the increase was greatly diminished in
322 cultures where Rab3A was present only in glia (KO on WT, CON, 15.2 $\pm$ 1.1 pA, TTX, 16.9 $\pm$ 0.7
323 pA). In the glial feeder layer culture, the loss of Rab3A in the neurons may have caused an
324 increase in mEPSC amplitude at baseline, similar to the Earlybird mutant in dissociated cultures,
325 but this difference was not significant (CON, WT on WT, 13.3 $\pm$ 0.5 pA; CON, KO on WT, 15.2 $\pm$

326 1.1 pA, p = 0.23, Kruskal-Wallis test), so it is also possible this can be attributed to culture to
327 culture variability. Regarding mEPSC frequency, in cultures with Rab3A$^{+/+}$ neurons, frequency
328 trended upward after activity blockade, whereas in the culture with Rab3A$^{-/-}$ neurons,
329 frequency was already increased (although not significantly, CON, WT on WT, 2.54 $\pm$ 0.57 sec^{-1};
330 CON, KO on WT, 4.46 $\pm$ 1.21 sec^{-1}, p = 0.23, Kruskal-Wallis test), and trended downward after
331 activity blockade.

332 In summary, in the absence of Rab3A from glia, the homeostatic plasticity of mEPSC
333 amplitude following activity blockade was normal, whereas in the absence of Rab3A in neurons,
334 homeostatic plasticity was greatly diminished. This result makes it highly unlikely that Rab3A is
335 required for the release of TNFα, or another factor from glia, that induces a homeostatic
336 upregulation of postsynaptic receptors and thereby increases mEPSC amplitude following TTX
337 treatment. Neuronal Rab3A appears to mediate the homeostatic increase in mEPSC amplitude
338 following activity blockade.

339

340 Discussion

341 We found that homeostatic synaptic plasticity of mEPSC amplitude in dissociated mixed
342 cultures of mouse cortical neurons and glia behaved remarkably similar to the mouse NMJ in
343 response to loss of Rab3A function: in cultures from Rab3A$^{-/-}$ mice, the increase in mEPSC
344 amplitudes following prolonged network silencing by TTX was strongly diminished, and in
345 cultures from Rab3A$^{Ebd/Ebd}$ mice, basal mEPSC amplitude was increased compared to that of
346 wild-type cultures and was not further modified by TTX treatment. These results suggest that

347 normal function of the synaptic vesicle protein Rab3A is required for the homeostatic increase
348 of mEPSC amplitude in cortical cultures. At the NMJ, the effect of Rab3A on homeostatic
349 upregulation of mEPC amplitude was not mediated by upregulation of postsynaptic receptors.
350 In neurons, the increase in mEPSC amplitude following block of activity was not due to
351 increases in Ca^{2+}-permeable GluA1 homomers because acute NASPM application was unable to
352 reverse the TTX-induced increase in amplitude. Imaging of immunofluorescence of GluA2
353 receptors revealed the response was more variable than that of mEPSC amplitude. The simplest
354 explanation for our findings at both the NMJ and in neurons is that Rab3A regulates a
355 presynaptic contributor to alteration of quantal amplitude during homeostatic synaptic
356 plasticity.

357

358 *Is the lack of homeostatic plasticity in the Earlybird mutant due to occlusion?*

359 We found that mEPSC amplitude was increased in untreated cultures prepared from
360 Rab3A$^{Ebd/Ebd}$ mice, compared to mEPSC amplitude in cultures from wild type mice. If there is a
361 limit to how large an mEPSC can become, it is possible that the mutant Rab3A does not affect
362 homeostatic plasticity, only occludes it. Similar increases in mEPSC amplitude at baseline,
363 combined with a failure to increase further after activity blockade, were noted in cultures
364 prepared from mECP2, AKAP, Homer1a, and Arc/Arg3.1 deletion mice (Shepherd et al., 2006;
365 Hu et al., 2010; Xu and Pozzo-Miller, 2017; Sanderson et al., 2018) as well as in cultures treated
366 with ubiquitin proteasome inhibitors (Jakawich et al., 2010) or microRNA 186-5p (Silva et al.,
367 2019), suggesting the possibility of a generalized phenomenon in which increased mEPSC

368 amplitude is induced when homeostatic regulation is disrupted. Since we did not observe such
369 an increase in mEPSC amplitude at baseline in cultures from Rab3A$^{-/-}$ mice, it remains a
370 possibility that the point mutant may bind to novel partners, causing activities that would not
371 be either facilitated or inhibited by Rab3A. Still, it is a strong coincidence that the novel activity
372 of the mutant Earlybird Rab3A would affect mEPSC amplitude, the same characteristic that is
373 modulated by activity blockade in a Rab3A dependent manner. Although we cannot rule out
374 occlusion, an alternate interpretation is that the presence of the mutant protein mimics the
375 condition of activity blockade.

376

377 *Homeostatic plasticity of postsynaptic receptors was less consistent than that of mEPSC*
378 *amplitude*

379 While we found that the effect of TTX treatment on mEPSC amplitude and GluA2
380 receptor levels were of similar magnitude, the effect on GluA2 receptor levels was not
381 statistically significant for the pooled data sets acquired in the same cultures, nor in a larger
382 data set containing 5 cultures. In light of the extensive literature documenting increases in
383 GluA1 or GluA2 receptors, or both, after activity blockade, the less than convincing increase in
384 GluA2 receptor levels in the current work came as a surprise. The reason for the lack of
385 significance was that the increase in receptors was more variable. We are aware of three
386 possible explanations for greater variability. 1) The number of synaptic sites sampled was
387 smaller for the imaging data set. This was because we limited our analysis to synaptic receptors
388 on the primary dendrite, where the increase in sensitivity to exogenously applied glutamate

389 was shown to be greatest (see Figure 3 in (Turrigiano et al., 1998)). To address this issue, we
390 limited our sample size of mEPSCs in the matched experiments to the same number per cell as
391 the mean sample size per cell for imaging, but there was still a discrepancy in the effect of TTX
392 on mEPSCs vs. receptors. 2) The small sample of only 3 cultures was not enough to reveal the
393 increase in receptors. We attempted to address this by adding 2 more cultures. Although both
394 additional cultures showed increases in GluA2 receptor cluster size, the magnitudes of the
395 increases were not large, and when cells from these cultures were included in the pooled data
396 set, the p value was not substantially improved. The only remaining possibility is: 3) The
397 complexity involved in processing cultures for immunofluorescence introduces variability that
398 obscures the true effect. One can get around technical issues related to immunofluorescence
399 processing by performing Western blots, but then any changes detected could be due to
400 upregulation of extrasynaptic receptors. What remains unclear is why our data were impacted
401 by this but data of other studies were not. Some other studies have used the number of
402 synaptic sites or puncta as the sample size (for example, (Hou et al., 2008; Ibata et al., 2008;
403 Wang et al., 2019)). When we analyzed our data after including as few as 6 randomly selected
404 cluster size measurements per cell, a Kruskal-Wallis test gave highly significant p values for 3
405 cultures ($p = 0.001$, $n = 174$ sites (6 *29 cells)) and 5 cultures ($p = 0.005$, $n = 294$ sites (6 *49
406 cells)). We found only a single study that had comparable sample sizes for receptors and
407 mEPSC amplitudes, and the p value was < 0.01 for mEPSC amplitudes ($n = 9$ and 10 cells for
408 CON and TTX, respectively), but five times higher (< 0.05) for receptor data ($n = 13$ and 14 cells
409 for CON and TTX) (Xu and Pozzo-Miller, 2017). This single example is consistent with our
410 suggestion that measurements of changes in receptors after activity blockade are more variable

411 than measurements of mEPSC amplitudes. In sum, our data suggest that TTX treatment of
412 mouse cortical cultures consistently leads to an increase in mEPSC amplitudes, and sometimes
413 leads to an increase in synaptic GluA2 receptor cluster size. Increased receptors likely
414 contribute to increases in mEPSC amplitudes, but our current data, coupled with our previous
415 findings at the mouse neuromuscular junction, support the idea that there are additional
416 sources contributing to the homeostatic increase in quantal size.
417
418 *Neuronal, not glial, Rab3A is required for homeostatic regulation of quantal amplitude*
419 Astrocytic release of TNFα was shown to mediate the increase in mEPSC amplitudes in
420 prolonged TTX-treated cultures of dissociated hippocampal neurons and cultures of
421 hippocampal slices (Stellwagen and Malenka, 2006; Heir et al., 2024), but we found that loss of
422 Rab3A in glia did not disrupt the increase in mEPSC amplitude after activity blockade. Further,
423 we previously showed that the homeostatic increase in NMJ mEPC amplitude was completely
424 normal in the absence of TNFα (Wang et al., 2011). This leaves neuronal Rab3A as the potential
425 controller of homeostatic regulation of quantal amplitude.
426
427 *Is Rab3A acting in the presynaptic cell to cause homeostatic increase in mEPSC amplitude?*
428 Our current results support the surprising possibility that the presynaptic vesicle protein
429 Rab3A either regulates postsynaptic AMPARs or regulates a presynaptic contributor to
430 homeostatic synaptic plasticity. To our knowledge, there is no evidence localizing Rab3A to
431 postsynaptic dendritic sites. Other presynaptic molecules, such as SNARE proteins,
432 synaptotagmins, and NSF, have been identified in the postsynaptic compartment (Lledo et al.,

433 1998; Nishimune et al., 1998; Osten et al., 1998; Song et al., 1998; Araki et al., 2010; Kennedy et
434 al., 2010; Suh et al., 2010; Jurado et al., 2013; Hussain and Davanger, 2015; Gu et al., 2016; Wu
435 et al., 2017). A recent report implicates Rab3A in the localization of plasma membrane proteins,
436 including the EGF receptor, in rafts in HEK cells and Jurkat-T cells, which indicates Rab3A can be
437 found in other specialized locations besides the presynaptic nerve terminal (Diaz-Rohrer et al.,
438 2023). Without additional experiments targeting Rab3A deletion to the pre- or post-synaptic
439 compartment, we cannot rule out that Rab3A is regulating homeostatic plasticity in mouse
440 cortical cultures by acting postsynaptically on receptor trafficking. However, given our previous
441 finding of a lack of any increase in AChR after TTX treatment the NMJ (Wang et al., 2011), the
442 simplest interpretation is that in these two situations, Rab3A is required for an increase in the
443 presynaptic quantum rather than an increase in postsynaptic receptors.

444 The presynaptic quantum, or the amount of transmitter released during a single fusion
445 event, is an important contributor to quantal size. The amount of transmitter released during
446 vesicle fusion can be affected by the kinetics of the fusion pore opening (Chang et al., 2017).
447 We previously used amperometric measurements in mouse adrenal chromaffin cells to show
448 loss of Rab3A increased the occurrence of very small amplitude fusion pore feet (Wang et al.,
449 2008). Paired with our finding that there is an increase in the occurrence of very slow-rising,
450 abnormally shaped mEPCs at the neuromuscular junction of Rab3A$^{-/-}$ mice, our data suggest
451 that small synaptic vesicles may have a fusion pore step under certain circumstances (see also
452 (Chiang et al., 2018)). If activity blockade causes an increase in mEPSC amplitude due to a more
453 rapid opening of a fusion pore, or a larger fusion pore conductance, it is possible that Rab3A is
454 required for this modulation.

455 Another way to increase the presynaptic quantum is to increase levels of the transmitter
456 transporter (Daniels et al., 2004; De Gois et al., 2005; Wilson et al., 2005; Hartman et al., 2006).
457 However, we found that immunofluorescence for the glutamate transporter, VGLUT1, was not
458 increased after activity blockade under our experimental conditions. A similar lack of increase in
459 VGLUT1 levels, relative to synapsin, was previously observed in hippocampal cultures treated
460 with NBQX, an AMPA receptor blocker (see supplemental data, (Wilson et al., 2005)). Taken
461 together with our findings, it appears that there is not strong evidence that the amount of
462 VGLUT1 at synapses is a contributing factor to the increase in mEPSC amplitude in neuronal
463 cultures after activity blockade with TTX.

464 Finally, the amount of transmitter released by a vesicle could be increased due to larger
465 vesicle size. Larger vesicle diameter has been observed following activity disruption in multiple
466 paradigms, including ocular deprivation, cortical ablation, and immobilization (Kawana et al.,
467 1971; Lloret and Saavedra, 1975; Cheresharov et al., 1978). Loss of Rab3 family members is
468 associated with increased vesicle size (Riedel et al., 2002; Schonn et al., 2010). Finally, an
469 increase in volume has been shown to increase miniature endplate junctional current
470 amplitude at the Drosophila NMJ (Karunanithi et al., 2002). Rab3A could be required for an
471 activity-dependent increase in vesicle size, but the increase in diameter needed for a 25%
472 increase in transmitter, and therefore mEPSC amplitude, would be difficult to detect.

473 The number of molecules shown to be required for homeostatic synaptic plasticity of
474 quantal size in neuronal cultures may have surpassed ~20 (see (Koesters et al., 2024) for a
475 recent summary), but fall into two main categories: molecules involved in glutamate receptor
476 expression or trafficking, and signaling molecules. To our knowledge, this is the first evidence

477 that a presynaptic protein is participating in this process. Homeostatic synaptic plasticity is
478 becoming increasingly implicated in essential normal functions such as sleep (Tononi and Cirelli,
479 2014; Diering et al., 2017; Torrado Pacheco et al., 2021), and pathological conditions such as
480 epilepsy, neuropsychiatric disorders, Huntington's, and alcohol use disorder (Trasande and
481 Ramirez, 2007; Fernandes and Carvalho, 2016; Wang et al., 2017; Lovinger and Abrahao, 2018;
482 Smith-Dijak et al., 2019; Lignani et al., 2020; Suzuki et al., 2021; Kavalali and Monteggia, 2023).
483 Therefore, our identification of a novel Rab3A-dependent regulatory pathway in homeostatic
484 synaptic plasticity may have important therapeutic implications. Our findings also further
485 cement the importance of Rab3A in activity-dependent modulation of synaptic strength.

486

487 Materials and Methods

488 *Animals.* To determine the role of Rab3A in homeostatic plasticity in mouse cortical cultures,
489 we employed two distinct genetic mouse strains with altered Rab3A function. Rab3A deletion
490 mice were generated as follows: Rab3A$^{+/-}$ heterozygous mice were bred and genotyped as
491 previously described (Kapfhamer et al., 2002; Wang et al., 2008), and maintained as a colony
492 using multiple heterozygous breeding pairs. Homozygous Rab3A$^{+/+}$ or Rab3A$^{-/-}$ mouse pups
493 were obtained by breeding Rab3A$^{+/+}$ pairs and Rab3A$^{-/-}$ pairs, respectively, so that the pups
494 were the first-generation progeny of a homozygous mating. This protocol minimizes the
495 tendency of multiple generations of Rab3A$^{+/+}$ and Rab3A$^{-/-}$ homozygous breedings to produce
496 progeny that are more and more genetically distinct. Rab3A$^{Ebd/Ebd}$ mice were identified in an
497 EU-mutagenesis screen of C57BL/6J mice, and after a cross to C3H/HeJ, were backcrossed for 3
498 generations to C57BL/6J (Kapfhamer et al., 2002). Rab3A$^{+/Ebd}$ heterozygous mice were bred at

499 Wright State University and genotyped in a two-step procedure: 1. a PCR reaction (forward
500 primer: TGA CTC CTT CAC TCC AGC CT; reverse primer: TGC ACT GCA TTA AAT GAC TCC T)
501 followed by 2. a restriction digest with enzyme Bsp1286I (New England Biolabs) that
502 distinguishes the Earlybird mutant by its different base-pair products. Rab3A$^{+/-}$ mice were
503 backcrossed with Rab3A$^{+/+}$ mice from the Earlybird heterozygous colony for 11 generations in
504 an attempt to establish a single wild type strain, but differences in mEPSC amplitude and
505 adrenal chromaffin cell calcium currents persisted, likely due to genes that are close to the
506 Rab3A site, resulting in two wild type strains: 1. Rab3A$^{+/+}$ from the Rab3A$^{+/-}$ colony, and 2.
507 Rab3A$^{+/+}$ from the Rab3A$^{+/Ebd}$ colony.

508 *Primary Culture of Mouse Cortical Neurons.* Primary dissociated cultures of mixed neuronal and
509 glia populations were prepared as previously described (Hanes et al., 2020). Briefly, postnatal
510 day 0-2 (P0-P2) Rab3A$^{+/+}$, Rab3A$^{-/-}$ or Rab3A$^{Ebd/Ebd}$ neonates were euthanized by rapid
511 decapitation, as approved by the Wright State University Institutional Animal Care and Use
512 Committee, and brains were quickly removed. Each culture was prepared from the cortices
513 harvested from two animals; neonates were not sexed. Cortices were collected in chilled
514 Neurobasal-A media (Gibco) with osmolarity adjusted to 270 mOsm and supplemented with 40
515 U/ml DNAse I (ThermoFisher Scientific). The tissues were digested with papain (Worthington
516 Biochemical) at 20 U/ml at 37°C for 20 minutes followed by trituration with a sterile, fire-
517 polished Pasteur pipette, then filtered through a 100 μm cell strainer, and centrifuged at 1100
518 rpm for 2 minutes. After discarding the supernatant, the pellet was resuspended in room
519 temperature Neurobasal-A media (270 mOsm), supplemented with 5% fetal bovine serum for
520 glia growth, and 2% B-27 supplement to promote neuronal growth (Gibco), L-glutamine, and

521 gentamicin (ThermoFisher Scientific). Neurons were counted and plated at 0.15 * 10^6
522 cells/coverslip onto 12 mm coverslips pre-coated with poly-L-lysine (BioCoat, Corning). This
523 plating density produces a "high density" culture characterized by a complex mesh of neuronal
524 processes criss-crossing the field of view, completely filling the space between cell bodies (see
525 Figure 4). We found in preliminary experiments that an increase in mEPSC amplitude in mouse
526 cortical cultures was inconsistent when cell density was low, likely due to lower levels of
527 baseline activity, although it is a limitation of this study that we did not directly measure activity
528 levels in cultures prepared from Rab3A$^{+/+}$, Rab3A$^{-/-}$ or Rab3A$^{Ebd/Ebd}$ mice, and therefore do not
529 know if differences in results are due to differences in activity levels. While unlikely for Rab3A$^{+/+}$
530 and Rab3A$^{-/-}$ studies, given the mEPSC amplitude in untreated cultures was relatively small, it
531 remains possible that in Rab3A$^{Ebd/Ebd}$ studies, the larger mEPSC amplitude in untreated cultures
532 was due to a loss of activity in these cultures. The culture media for the first day (0 DIV) was the
533 same as the above Neurobasal-A media supplemented with FBS, B-27, L-glutamine, and
534 gentamicin, and was switched after 24 hours (1 DIV) to media consisting of Neurobasal-A (270
535 mOsm), 2% B-27, and L-glutamine without FBS to avoid its toxic effects on neuronal viability
536 and health (Stellwagen and Malenka, 2006). Half of the media was changed twice weekly and
537 experiments were performed at 13-14 DIV. Two days prior to experiments, tetrodotoxin (TTX)
538 (500 nM; Tocris), a potent Na^+ channel blocker, was added to some cultures to chronically
539 silence all network activity and induce homeostatic synaptic plasticity mechanisms, while
540 untreated sister cultures served as controls. Cultures prepared from mutant mice were
541 compared with cultures from wild-type mice from their respective colonies. Note that the
542 cultures comprising the Rab3A$^{+/+}$ data here are a subset of the data previously published in

543 Hanes et al., 2020. This smaller data set was restricted to the time period over which cultures
544 were also prepared from Rab3A$^{-/-}$ mice.

545 *Preparation of Glial Feeder Layers.* Glial feeder layers were prepared from the cortices of P0-P2
546 Rab3A$^{+/+}$ or Rab3A$^{-/-}$ mouse pups as described previously (Stellwagen and Malenka, 2006).
547 Briefly, cortices were dissected and cells were dissociated as described above. Cell suspensions
548 of mixed neuronal and glial populations were plated onto glass coverslips pre-coated with poly-
549 L-lysine in Dulbecco's Modified Eagle Media (ThermoFisher Scientific) supplemented with 5%
550 FBS (to promote glial proliferation and to kill neurons), L-glutamine, and gentamicin, and
551 maintained in an incubator at 37°C, 5% CO_2; cultures were maintained in this manner for up to
552 1 month to generate purely glial cultures (all neurons typically died off by 7 DIV). Culture media
553 was replaced after 24 hours, and subsequent media changes were made twice weekly,
554 replacing half of the culture media with fresh media. Feeder layers were not used for neuronal
555 seeding until all native neurons were gone and glia approached 100% confluency (visually
556 inspected).

557 *Plating of Neurons on Glial Feeder Layers.* Cortical neurons were obtained as described above.
558 The cell pellet obtained was resuspended in Neurobasal-A (osmolarity adjusted to 270 mOsm)
559 containing B27 (2%, to promote neuronal growth), L-glutamine, and 5-fluorodeoxyuridine (FdU,
560 a mitotic inhibitor; Sigma). Addition of FdU was used to prevent glial proliferation and
561 contamination of the feeder layer with new glia, promoting only neuronal growth on the feeder
562 layers (FdU-containing media was used for the maintenance of these cultures and all
563 subsequent media changes). Glial culture media was removed from the feeder layer cultures,
564 and the neuronal cell suspension was plated onto the glial feeder cultures. The culture strategy

565 used to distinguish the relative roles of neuronal and glial Rab3A is outlined in Figure 8, Left. At
566 1 DIV, all of the culture media was removed and replaced with fresh Neurobasal-A media
567 containing FdU described above, and half of the media was replaced twice per week for all
568 subsequent media changes. Cultures were maintained in a 37°C, 5% CO_2 incubator for 13-14
569 DIV.

570 *Whole-Cell Voltage Clamp to Record mEPSCs*. At 13-14 DIV, mEPSCs from TTX-treated and
571 untreated sister cultures of Rab3A$^{+/+}$ or Rab3A$^{-/-}$ neurons from the Rab3A$^{+/-}$ colony, or Rab3A$^{+/+}$
572 or Rab3A$^{Ebd/Ebd}$ neurons from the Rab3A$^{+/Ebd}$ colony, were recorded via whole-cell voltage clamp
573 to assess the role of Rab3A in homeostatic synaptic plasticity. Recordings were taken from
574 pyramidal neurons, which were identified visually by a prominent apical dendrite; images were
575 taken of all cells recorded from. Cells were continuously perfused with a solution consisting of
576 (in mM): NaCl (115), KCl (5), $CaCl_2$ (2.5), $MgCl_2$ (1.3), dextrose (23), sucrose (26), HEPES (4.2),
577 pH = 7.2 (Stellwagen and Malenka, 2006). On the day of recording, the osmolarity of the media
578 from the cultures was measured (normally 285 – 295 mOsm) and the perfusate osmolarity was
579 adjusted to match the culture osmolarity to protect against osmotic shock to the neurons. To
580 isolate glutamatergic mEPSCs, TTX (500 nM) and picrotoxin (50 µM), were included in the
581 perfusion solution to block action potentials and GABAergic currents, respectively. The NMDA
582 receptor antagonist, APV, was not included in the perfusion solution because in pilot studies, all
583 mEPSCs were blocked by 10 µM CNQX and 50 µm picrotoxin, demonstrating no APV-sensitive
584 mEPSCs were present (data not shown). Previous studies have described NMDA mEPSCs in
585 neuronal cultures, but recordings were performed in 0 Mg^{2+} (Watt et al., 2000; Sutton et al.,
586 2006). In our recordings, the presence of extracellular Mg^{2+} (1.3 mM) <u>and</u> TTX would mean that

587 the majority of NMDA receptors are blocked by extracellular Mg^{2+} at resting Vm. Patch
588 electrodes (3.5 – 5 MΩ) were filled with an internal solution containing (in mM): K-gluconate
589 (130), NaCl (10), EGTA (1), $CaCl_2$ (0.132), $MgCl_2$ (2), HEPES (10), pH = 7.2. Osmolarity was
590 adjusted to 10 mOsm less than the perfusion solution osmolarity, which we have found
591 improves success rate of achieving low access resistance recordings. Neurons were clamped at
592 a voltage of -60 mV using an Axopatch 200B patch-clamp (Axon Instruments), recorded from for
593 2 – 5 minutes, and data were collected with Clampex 10.0/10.2 (Axon Instruments).
594
595 *NASPM application*. The antagonist of Ca^{2+}-permeable AMPA receptors, N-naphthyl
596 acetylspermine (NASPM, 20 μM; Tocris), was applied during recordings in a subset of
597 experiments. NASPM is a synthetic analog of Joro Spider Toxin (JSTX) (Koike et al., 1997), and
598 chemicals in this family block Ca^{2+} permeable glutamate receptors (Blaschke et al., 1993;
599 Herlitze et al., 1993; Iino et al., 1996). The presence of the edited GluA2 subunit disrupts both
600 the Ca^{2+} permeability and the sensitivity to JSTX and related substances (Blaschke et al., 1993;
601 Bochet et al., 1994; Jonas and Burnashev, 1995). Therefore, 20 μM NASPM is expected to
602 completely block AMPA receptors containing GluA1, GluA3 or GluA4 subunits (Hollmann et al.,
603 1991; Burnashev et al., 1992), or the Kainate receptors containing GluA5 or GluA6 (Koike et al.,
604 1997; Sun et al., 2009), but be ineffective against any heteromer or homomer containing GluA2
605 subunits. Because the effect of the spider toxins and their analogues are use-dependent
606 (Herlitze et al., 1993; Iino et al., 1996; Koike et al., 1997), NASPM was applied with a
607 depolarizing high K^+ solution (25 mM KCl, 95 mM NaCl) which we expected to trigger release of
608 glutamate and opening of glutamate-activated receptors, allowing entry of NASPM into the

609 pore. Baseline recordings were performed for 2 minutes in our standard perfusate, followed by
610 perfusion of NASPM + High K^+ solution for 45 seconds, and then perfusion of a NASPM only
611 solution for 5 minutes, after which recording was recommenced for 5 minutes (because we
612 found in pilot experiments that frequency was reduced following NASPM application).
613 *Analysis of mEPSCs.* Miniature excitatory postsynaptic currents (mEPSCs) were manually
614 selected using Mini Analysis software (Synaptosoft), a standard program used for mEPSC event
615 detection and analysis. Records were filtered at 2 kHz using a low-pass Butterworth filter prior
616 to selection. The program detection threshold was set at 3 pA but the smallest mEPSC selected
617 was 4.01 pA. A fully manual detection process means that the same criterion ("does this *look*
618 like an mEPSC?") is applied to all events, not just the false positives or the false negatives,
619 which prevents the bias from being primarily at one end or the other of the range of mEPSC
620 amplitudes. It is important to note that when performing the MiniAnalysis process, the
621 researcher did not know whether a record was from an untreated cell or a TTX-treated cell.
622 *Immunofluorescence, microscopy, and data analysis.* Primary cultures of mouse cortical
623 neurons were grown for 13-14 DIV. Antibodies to GluA2 (mouse ab against N-terminal, EMD
624 Millipore) were added directly to live cultures at 1:40 dilution, and incubated at 37 °C in a CO_2
625 incubator for 45 minutes. Cultures were rinsed 3 times with PBS/5% donkey serum before being
626 fixed with 4% paraformaldehyde. After 3 rinses in PBS/5% donkey serum, cultures were
627 incubated in CY3-labeled donkey-anti-mouse secondary antibodies for 1 hour at room
628 temperature, rinsed in PBS/5% donkey serum, permeabilized with 0.2% saponin, and incubated
629 in chick anti-MAP2 (1:2500, AbCAM) and rabbit anti-VGLUT1 (1:4000, Synaptic Systems) for 1
630 hour at room temperature in PBS/5% donkey serum. After rinsing with PBS/5% donkey serum,

631 coverslips were incubated with 488-anti chick and CY5-anti rabbit secondary antibodies for 1
632 hour at room temperature, rinsed, blotted to remove excess liquid, and inverted on a drop of
633 Vectashield (Vector Labs). Coverslips were sealed with nail polish and stored at 4 °C for < 1
634 week before imaging. All secondary antibodies were from Jackson Immunoresearch and were
635 used at 1:225 dilution.

636 Coverslips were viewed on a Fluoview FV1000 laser scanning confocal microscope with a
637 60x oil immersion, 1.35 NA objective. Once a pyramidal neuron was identified and a single
638 confocal section of the cell acquired (see Top, Figure 4), Fluoview 2.1 software was used to
639 zoom in on the primary dendrite (5X) and a series of confocal sections were taken every 0.5
640 μm. Images were analyzed offline with ImagePro 6 (Cybernetics). The composite image was
641 used to locate synaptic sites containing both VGLUT1 and GluA2 immunoreactivity in close
642 apposition to each other and to the primary dendrite or a secondary branch identified with
643 MAP2 immunoreactivity. An area of interest (AOI) was manually drawn around the GluA2
644 cluster in the confocal section in which it was the brightest. The AOIs for a dendrite were saved
645 in a single file; the AOI number and the confocal section it was associated with were noted for
646 later retrieval. For quantification, AOIs were loaded, an individual AOI was called up on the
647 appropriate section, and the count/measurement tool used to apply a threshold. Multiple
648 thresholds were used, 400-550, but we found that within a given experiment, the magnitude of
649 the TTX effect was not altered by different thresholds, therefore, all data presented here use a
650 threshold of 450. Pixels within the cluster that were above the threshold were automatically
651 outlined, and size, average intensity, and integral of the outlined region saved to Origin2020
652 (OriginLab) file for calculating mean values. For analyzing VGLUT1 sites, previous AOIs were

653 examined, and if not directly over the VGLUT1 site, moved to encompass it (this happened
654 when GluA2 and VGLUT1 were side by side rather than overlapping). The threshold was 200 for
655 all VGLUT1 data except Rab3A$^{+/+}$ Culture #1, where threshold was 400. There was no threshold
656 that worked for both that culture and the other cultures, with too much of the background
657 regions being included for Culture #1 with a threshold of 200, and too little of the synaptic site
658 area being included for the other Cultures with a threshold of 400.

659 *Statistics.* In our previous publication (Hanes et al., 2020), we described the characteristics of
660 homeostatic plasticity of mEPSC amplitudes in mouse cortical cultures using multiple mEPSC
661 amplitude quantiles from each cell to create data sets with thousands of samples. We
662 compared the cumulative distribution functions for mEPSC amplitudes in untreated vs. TTX-
663 treated cultures, as well as sorting the values from smallest to largest, and plotted TTX values
664 vs. control values in the rank order plot first described in (Turrigiano et al., 1998) to
665 demonstrate synaptic scaling. Finally, we plotted the ratio of TTX values/control values vs.
666 control values to show that the ratio, which represents the effect of TTX, increased with
667 increasing control values, which we termed "divergent scaling." Here, we wanted to avoid the
668 inflation of sample size caused by pooling multiple mEPSCs per cell in order to statistically
669 compare the effects of TTX in cultures of wild type mice, Rab3A$^{-/-}$ mice and Rab3A$^{Ebd/Ebd}$ mutant
670 mice. Therefore, we computed the mean mEPSC amplitude for each cell and compared means
671 from untreated and TTX-treated cultures with the non-parametric Kruskal-Wallis test, with N =
672 the number of cells. The overall means are presented ± SEM in the text, and p values are
673 displayed above each plot. The same process was carried out for the characteristics of synaptic
674 GluA2 receptor clusters and VGLUT1 sites in imaging experiments, with N = the number of

675 dendrites (one dendrite was sampled for each cell). Although we quantified three
676 characteristics of the GluA2 clusters and VGLUT1 sites, size, average intensity, and integral, we
677 have not corrected p values for multiple comparisons. Means are presented as box plots + data,
678 with the box at 25 and 75 percentiles, whiskers at 10 and 90 percentiles, a dot indicating the
679 mean, and a line indicating the median. In Figure 3, mEPSC amplitudes were measured within
680 the same cell before and after NASPM application, so a paired t test was used to compare the
681 pre- and post-NASPM mEPSC amplitudes. In Figure 5A-C the mean mEPSC amplitude for
682 untreated and TTX-treated coverslips in the same culture are compared with a paired t test.
683 Statistics were computed and plots were created using Origin2020 (OriginLab).
684
685

686

687 References

688

689 Araki Y, Lin DT, Huganir RL (2010) Plasma membrane insertion of the AMPA receptor GluA2 subunit is
690 regulated by NSF binding and Q/R editing of the ion pore. Proc Natl Acad Sci U S A 107:11080-
691 11085.
692 Blaschke M, Keller BU, Rivosecchi R, Hollmann M, Heinemann S, Konnerth A (1993) A single amino acid
693 determines the subunit-specific spider toxin block of alpha-amino-3-hydroxy-5-methylisoxazole-
694 4-propionate/kainate receptor channels. Proc Natl Acad Sci U S A 90:6528-6532.
695 Bochet P, Audinat E, Lambolez B, Crepel F, Rossier J, Iino M, Tsuzuki K, Ozawa S (1994) Subunit
696 composition at the single-cell level explains functional properties of a glutamate-gated channel.
697 Neuron 12:383-388.
698 Burnashev N, Monyer H, Seeburg PH, Sakmann B (1992) Divalent ion permeability of AMPA receptor
699 channels is dominated by the edited form of a single subunit. Neuron 8:189-198.
700 Castillo PE, Janz R, Sudhof TC, Tzounopoulos T, Malenka RC, Nicoll RA (1997) Rab3A is essential for
701 mossy fibre long-term potentiation in the hippocampus. Nature 388:590-593.
702 Chang CW, Chiang CW, Jackson MB (2017) Fusion pores and their control of neurotransmitter and
703 hormone release. J Gen Physiol 149:301-322.
704 Cheresharov L, Ovtscharoff W, Manolov S (1978) Ultrastructural changes in the anterior horn synapses
705 of rat spinal cord under different locomotor conditions. J Neural Transm 42:9-21.
706 Chiang CW, Chang CW, Jackson MB (2018) The Transmembrane Domain of Synaptobrevin Influences
707 Neurotransmitter Flux through Synaptic Fusion Pores. J Neurosci 38:7179-7191.
708 Coleman WL, Bykhovskaia M (2009) Rab3a-mediated vesicle recruitment regulates short-term plasticity
709 at the mouse diaphragm synapse. Mol Cell Neurosci 41:286-296.
710 Coleman WL, Bykhovskaia M (2010) Cooperative regulation of neurotransmitter release by Rab3a and
711 synapsin II. Mol Cell Neurosci 44:190-200.
712 Coleman WL, Bill CA, Bykhovskaia M (2007) Rab3a deletion reduces vesicle docking and transmitter
713 release at the mouse diaphragm synapse. Neuroscience 148:1-6.
714 Daniels RW, Collins CA, Gelfand MV, Dant J, Brooks ES, Krantz DE, DiAntonio A (2004) Increased
715 expression of the Drosophila vesicular glutamate transporter leads to excess glutamate release
716 and a compensatory decrease in quantal content. J Neurosci 24:10466-10474.
717 De Gois S, Schafer MK, Defamie N, Chen C, Ricci A, Weihe E, Varoqui H, Erickson JD (2005) Homeostatic
718 scaling of vesicular glutamate and GABA transporter expression in rat neocortical circuits. J
719 Neurosci 25:7121-7133.
720 Diaz-Rohrer B, Castello-Serrano I, Chan SH, Wang HY, Shurer CR, Levental KR, Levental I (2023) Rab3
721 mediates a pathway for endocytic sorting and plasma membrane recycling of ordered
722 microdomains. Proc Natl Acad Sci U S A 120:e2207461120.
723 Diering GH, Nirujogi RS, Roth RH, Worley PF, Pandey A, Huganir RL (2017) Homer1a drives homeostatic
724 scaling-down of excitatory synapses during sleep. Science 355:511-515.
725 Dubes S, Soula A, Benquet S, Tessier B, Poujol C, Favereaux A, Thoumine O, Letellier M (2022) miR-124-
726 dependent tagging of synapses by synaptopodin enables input-specific homeostatic plasticity.
727 EMBO J 41:e109012.

728 Fan D, Grooms SY, Araneda RC, Johnson AB, Dobrenis K, Kessler JA, Zukin RS (1999) AMPA receptor
729 protein expression and function in astrocytes cultured from hippocampus. J Neurosci Res
730 57:557-571.
731 Fernandes D, Carvalho AL (2016) Mechanisms of homeostatic plasticity in the excitatory synapse. J
732 Neurochem 139:973-996.
733 Geppert M, Bolshakov VY, Siegelbaum SA, Takei K, De Camilli P, Hammer RE, Sudhof TC (1994) The role
734 of Rab3A in neurotransmitter release. Nature 369:493-497.
735 Gu Y, Chiu SL, Liu B, Wu PH, Delannoy M, Lin DT, Wirtz D, Huganir RL (2016) Differential vesicular sorting
736 of AMPA and GABAA receptors. Proc Natl Acad Sci U S A 113:E922-931.
737 Hanes AL, Koesters AG, Fong MF, Altimimi HF, Stellwagen D, Wenner P, Engisch KL (2020) Divergent
738 Synaptic Scaling of Miniature EPSCs following Activity Blockade in Dissociated Neuronal Cultures.
739 J Neurosci 40:4090-4102.
740 Hartman KN, Pal SK, Burrone J, Murthy VN (2006) Activity-dependent regulation of inhibitory synaptic
741 transmission in hippocampal neurons. Nat Neurosci 9:642-649.
742 Heir R, Abbasi Z, Komal P, Altimimi HF, Franquin M, Moschou D, Chambon J, Stellwagen D (2024)
743 Astrocytes Are the Source of TNF Mediating Homeostatic Synaptic Plasticity. J Neurosci 44.
744 Herlitze S, Raditsch M, Ruppersberg JP, Jahn W, Monyer H, Schoepfer R, Witzemann V (1993) Argiotoxin
745 detects molecular differences in AMPA receptor channels. Neuron 10:1131-1140.
746 Hollmann M, Hartley M, Heinemann S (1991) Ca2+ permeability of KA-AMPA--gated glutamate receptor
747 channels depends on subunit composition. Science 252:851-853.
748 Hong Y, Zhao T, Li XJ, Li S (2016) Mutant Huntingtin Impairs BDNF Release from Astrocytes by Disrupting
749 Conversion of Rab3a-GTP into Rab3a-GDP. J Neurosci 36:8790-8801.
750 Hou Q, Zhang D, Jarzylo L, Huganir RL, Man HY (2008) Homeostatic regulation of AMPA receptor
751 expression at single hippocampal synapses. Proc Natl Acad Sci U S A 105:775-780.
752 Hu JH, Park JM, Park S, Xiao B, Dehoff MH, Kim S, Hayashi T, Schwarz MK, Huganir RL, Seeburg PH,
753 Linden DJ, Worley PF (2010) Homeostatic scaling requires group I mGluR activation mediated by
754 Homer1a. Neuron 68:1128-1142.
755 Hussain S, Davanger S (2015) Postsynaptic VAMP/Synaptobrevin Facilitates Differential Vesicle
756 Trafficking of GluA1 and GluA2 AMPA Receptor Subunits. PLoS One 10:e0140868.
757 Ibata K, Sun Q, Turrigiano GG (2008) Rapid synaptic scaling induced by changes in postsynaptic firing.
758 Neuron 57:819-826.
759 Iino M, Koike M, Isa T, Ozawa S (1996) Voltage-dependent blockage of Ca(2+)-permeable AMPA
760 receptors by joro spider toxin in cultured rat hippocampal neurones. J Physiol 496 (Pt 2):431-
761 437.
762 Jakawich SK, Neely RM, Djakovic SN, Patrick GN, Sutton MA (2010) An essential postsynaptic role for the
763 ubiquitin proteasome system in slow homeostatic synaptic plasticity in cultured hippocampal
764 neurons. Neuroscience 171:1016-1031.
765 Jonas P, Burnashev N (1995) Molecular mechanisms controlling calcium entry through AMPA-type
766 glutamate receptor channels. Neuron 15:987-990.
767 Ju W, Morishita W, Tsui J, Gaietta G, Deerinck TJ, Adams SR, Garner CC, Tsien RY, Ellisman MH, Malenka
768 RC (2004) Activity-dependent regulation of dendritic synthesis and trafficking of AMPA
769 receptors. Nat Neurosci 7:244-253.
770 Jurado S, Goswami D, Zhang Y, Molina AJ, Sudhof TC, Malenka RC (2013) LTP requires a unique
771 postsynaptic SNARE fusion machinery. Neuron 77:542-558.
772 Kapfhamer D, Valladares O, Sun Y, Nolan PM, Rux JJ, Arnold SE, Veasey SC, Bucan M (2002) Mutations in
773 Rab3a alter circadian period and homeostatic response to sleep loss in the mouse. Nat Genet
774 32:290-295.

775 Karunanithi S, Marin L, Wong K, Atwood HL (2002) Quantal size and variation determined by vesicle size
776 in normal and mutant Drosophila glutamatergic synapses. J Neurosci 22:10267-10276.
777 Kavalali ET, Monteggia LM (2023) Rapid homeostatic plasticity and neuropsychiatric therapeutics.
778 Neuropsychopharmacology 48:54-60.
779 Kawana E, Akert K, Bruppacher H (1971) Enlargement of synaptic vesicles as an early sign of terminal
780 degneration in the rat caudate nucleus. J Comp Neurol 142:297-307.
781 Kennedy MJ, Davison IG, Robinson CG, Ehlers MD (2010) Syntaxin-4 defines a domain for activity-
782 dependent exocytosis in dendritic spines. Cell 141:524-535.
783 Koesters AG, Rich MM, Engisch KL (2024) Diverging from the Norm: Reevaluating What Miniature
784 Excitatory Postsynaptic Currents Tell Us about Homeostatic Synaptic Plasticity. Neuroscientist
785 30:49-70.
786 Koike M, Iino M, Ozawa S (1997) Blocking effect of 1-naphthyl acetyl spermine on Ca(2+)-permeable
787 AMPA receptors in cultured rat hippocampal neurons. Neurosci Res 29:27-36.
788 Leenders AG, Lopes da Silva FH, Ghijsen WE, Verhage M (2001) Rab3a is involved in transport of synaptic
789 vesicles to the active zone in mouse brain nerve terminals. Mol Biol Cell 12:3095-3102.
790 Lignani G, Baldelli P, Marra V (2020) Homeostatic Plasticity in Epilepsy. Front Cell Neurosci 14:197.
791 Lledo PM, Zhang X, Sudhof TC, Malenka RC, Nicoll RA (1998) Postsynaptic membrane fusion and long-
792 term potentiation. Science 279:399-403.
793 Lloret IL, Saavedra JP (1975) Enlargement of synaptic vesicles in degenerating nerve endings: a
794 comparison between cat and monkey. J Neurocytol 4:1-6.
795 Lonart G, Janz R, Johnson KM, Sudhof TC (1998) Mechanism of action of rab3A in mossy fiber LTP.
796 Neuron 21:1141-1150.
797 Lovinger DM, Abrahao KP (2018) Synaptic plasticity mechanisms common to learning and alcohol use
798 disorder. Learn Mem 25:425-434.
799 Maienschein V, Marxen M, Volknandt W, Zimmermann H (1999) A plethora of presynaptic proteins
800 associated with ATP-storing organelles in cultured astrocytes. Glia 26:233-244.
801 Nishimune A, Isaac JT, Molnar E, Noel J, Nash SR, Tagaya M, Collingridge GL, Nakanishi S, Henley JM
802 (1998) NSF binding to GluR2 regulates synaptic transmission. Neuron 21:87-97.
803 O'Brien RJ, Kamboj S, Ehlers MD, Rosen KR, Fischbach GD, Huganir RL (1998) Activity-dependent
804 modulation of synaptic AMPA receptor accumulation. Neuron 21:1067-1078.
805 Ormel L, Stensrud MJ, Bergersen LH, Gundersen V (2012) VGLUT1 is localized in astrocytic processes in
806 several brain regions. Glia 60:229-238.
807 Osten P, Srivastava S, Inman GJ, Vilim FS, Khatri L, Lee LM, States BA, Einheber S, Milner TA, Hanson PI,
808 Ziff EB (1998) The AMPA receptor GluR2 C terminus can mediate a reversible, ATP-dependent
809 interaction with NSF and alpha- and beta-SNAPs. Neuron 21:99-110.
810 Pozo K, Goda Y (2010) Unraveling mechanisms of homeostatic synaptic plasticity. Neuron 66:337-351.
811 Riedel D, Antonin W, Fernandez-Chacon R, Alvarez de Toledo G, Jo T, Geppert M, Valentijn JA, Valentijn
812 K, Jamieson JD, Sudhof TC, Jahn R (2002) Rab3D is not required for exocrine exocytosis but for
813 maintenance of normally sized secretory granules. Mol Cell Biol 22:6487-6497.
814 Sanderson JL, Scott JD, Dell'Acqua ML (2018) Control of Homeostatic Synaptic Plasticity by AKAP-
815 Anchored Kinase and Phosphatase Regulation of Ca(2+)-Permeable AMPA Receptors. J Neurosci
816 38:2863-2876.
817 Schluter OM, Basu J, Sudhof TC, Rosenmund C (2006) Rab3 superprimes synaptic vesicles for release:
818 implications for short-term synaptic plasticity. J Neurosci 26:1239-1246.
819 Schonn JS, van Weering JR, Mohrmann R, Schluter OM, Sudhof TC, de Wit H, Verhage M, Sorensen JB
820 (2010) Rab3 proteins involved in vesicle biogenesis and priming in embryonic mouse chromaffin
821 cells. Traffic 11:1415-1428.

822 Shepherd JD, Rumbaugh G, Wu J, Chowdhury S, Plath N, Kuhl D, Huganir RL, Worley PF (2006)
823 Arc/Arg3.1 mediates homeostatic synaptic scaling of AMPA receptors. Neuron 52:475-484.
824 Silva MM, Rodrigues B, Fernandes J, Santos SD, Carreto L, Santos MAS, Pinheiro P, Carvalho AL (2019)
825 MicroRNA-186-5p controls GluA2 surface expression and synaptic scaling in hippocampal
826 neurons. Proc Natl Acad Sci U S A 116:5727-5736.
827 Smith-Dijak AI, Nassrallah WB, Zhang LYJ, Geva M, Hayden MR, Raymond LA (2019) Impairment and
828 Restoration of Homeostatic Plasticity in Cultured Cortical Neurons From a Mouse Model of
829 Huntington Disease. Front Cell Neurosci 13:209.
830 Song I, Kamboj S, Xia J, Dong H, Liao D, Huganir RL (1998) Interaction of the N-ethylmaleimide-sensitive
831 factor with AMPA receptors. Neuron 21:393-400.
832 Stellwagen D, Malenka RC (2006) Synaptic scaling mediated by glial TNF-alpha. Nature 440:1054-1059.
833 Stellwagen D, Beattie EC, Seo JY, Malenka RC (2005) Differential regulation of AMPA receptor and GABA
834 receptor trafficking by tumor necrosis factor-alpha. J Neurosci 25:3219-3228.
835 Suh YH, Terashima A, Petralia RS, Wenthold RJ, Isaac JT, Roche KW, Roche PA (2010) A neuronal role for
836 SNAP-23 in postsynaptic glutamate receptor trafficking. Nat Neurosci 13:338-343.
837 Sun HY, Bartley AF, Dobrunz LE (2009) Calcium-permeable presynaptic kainate receptors involved in
838 excitatory short-term facilitation onto somatostatin interneurons during natural stimulus
839 patterns. J Neurophysiol 101:1043-1055.
840 Sutton MA, Ito HT, Cressy P, Kempf C, Woo JC, Schuman EM (2006) Miniature neurotransmission
841 stabilizes synaptic function via tonic suppression of local dendritic protein synthesis. Cell
842 125:785-799.
843 Suzuki K, Kim JW, Nosyreva E, Kavalali ET, Monteggia LM (2021) Convergence of distinct signaling
844 pathways on synaptic scaling to trigger rapid antidepressant action. Cell Rep 37:109918.
845 Tatavarty V, Sun Q, Turrigiano GG (2013) How to scale down postsynaptic strength. J Neurosci 33:13179-
846 13189.
847 Thiagarajan TC, Lindskog M, Tsien RW (2005) Adaptation to synaptic inactivity in hippocampal neurons.
848 Neuron 47:725-737.
849 Tian M, Xu CS, Montpetit R, Kramer RH (2012) Rab3A mediates vesicle delivery at photoreceptor ribbon
850 synapses. J Neurosci 32:6931-6936.
851 Tononi G, Cirelli C (2014) Sleep and the price of plasticity: from synaptic and cellular homeostasis to
852 memory consolidation and integration. Neuron 81:12-34.
853 Torrado Pacheco A, Bottorff J, Gao Y, Turrigiano GG (2021) Sleep Promotes Downward Firing Rate
854 Homeostasis. Neuron 109:530-544 e536.
855 Trasande CA, Ramirez JM (2007) Activity deprivation leads to seizures in hippocampal slice cultures: is
856 epilepsy the consequence of homeostatic plasticity? J Clin Neurophysiol 24:154-164.
857 Turrigiano GG, Nelson SB (2004) Homeostatic plasticity in the developing nervous system. Nat Rev
858 Neurosci 5:97-107.
859 Turrigiano GG, Leslie KR, Desai NS, Rutherford LC, Nelson SB (1998) Activity-dependent scaling of
860 quantal amplitude in neocortical neurons. Nature 391:892-896.
861 Wang G, Zhong J, Guttieres D, Man HY (2019) Non-scaling regulation of AMPA receptors in homeostatic
862 synaptic plasticity. Neuropharmacology 158:107700.
863 Wang JKT, Langfelder P, Horvath S, Palazzolo MJ (2017) Exosomes and Homeostatic Synaptic Plasticity
864 Are Linked to Each other and to Huntington's, Parkinson's, and Other Neurodegenerative
865 Diseases by Database-Enabled Analyses of Comprehensively Curated Datasets. Front Neurosci
866 11:149.
867 Wang X, Thiagarajan R, Wang Q, Tewolde T, Rich MM, Engisch KL (2008) Regulation of quantal shape by
868 Rab3A: evidence for a fusion pore-dependent mechanism. J Physiol 586:3949-3962.

869 Wang X, Wang Q, Yang S, Bucan M, Rich MM, Engisch KL (2011) Impaired activity-dependent plasticity of
870 quantal amplitude at the neuromuscular junction of Rab3A deletion and Rab3A earlybird mutant
871 mice. J Neurosci 31:3580-3588.
872 Wang X, Li Y, Engisch KL, Nakanishi ST, Dodson SE, Miller GW, Cope TC, Pinter MJ, Rich MM (2005)
873 Activity-dependent presynaptic regulation of quantal size at the mammalian neuromuscular
874 junction in vivo. J Neurosci 25:343-351.
875 Watt AJ, van Rossum MC, MacLeod KM, Nelson SB, Turrigiano GG (2000) Activity coregulates quantal
876 AMPA and NMDA currents at neocortical synapses. Neuron 26:659-670.
877 Weisskopf MG, Castillo PE, Zalutsky RA, Nicoll RA (1994) Mediation of hippocampal mossy fiber long-
878 term potentiation by cyclic AMP. Science 265:1878-1882.
879 Wierenga CJ, Ibata K, Turrigiano GG (2005) Postsynaptic expression of homeostatic plasticity at
880 neocortical synapses. J Neurosci 25:2895-2905.
881 Wilson NR, Kang J, Hueske EV, Leung T, Varoqui H, Murnick JG, Erickson JD, Liu G (2005) Presynaptic
882 regulation of quantal size by the vesicular glutamate transporter VGLUT1. J Neurosci 25:6221-
883 6234.
884 Wu D, Bacaj T, Morishita W, Goswami D, Arendt KL, Xu W, Chen L, Malenka RC, Sudhof TC (2017)
885 Postsynaptic synaptotagmins mediate AMPA receptor exocytosis during LTP. Nature 544:316-
886 321.
887 Xu X, Pozzo-Miller L (2017) EEA1 restores homeostatic synaptic plasticity in hippocampal neurons from
888 Rett syndrome mice. J Physiol 595:5699-5712.

889

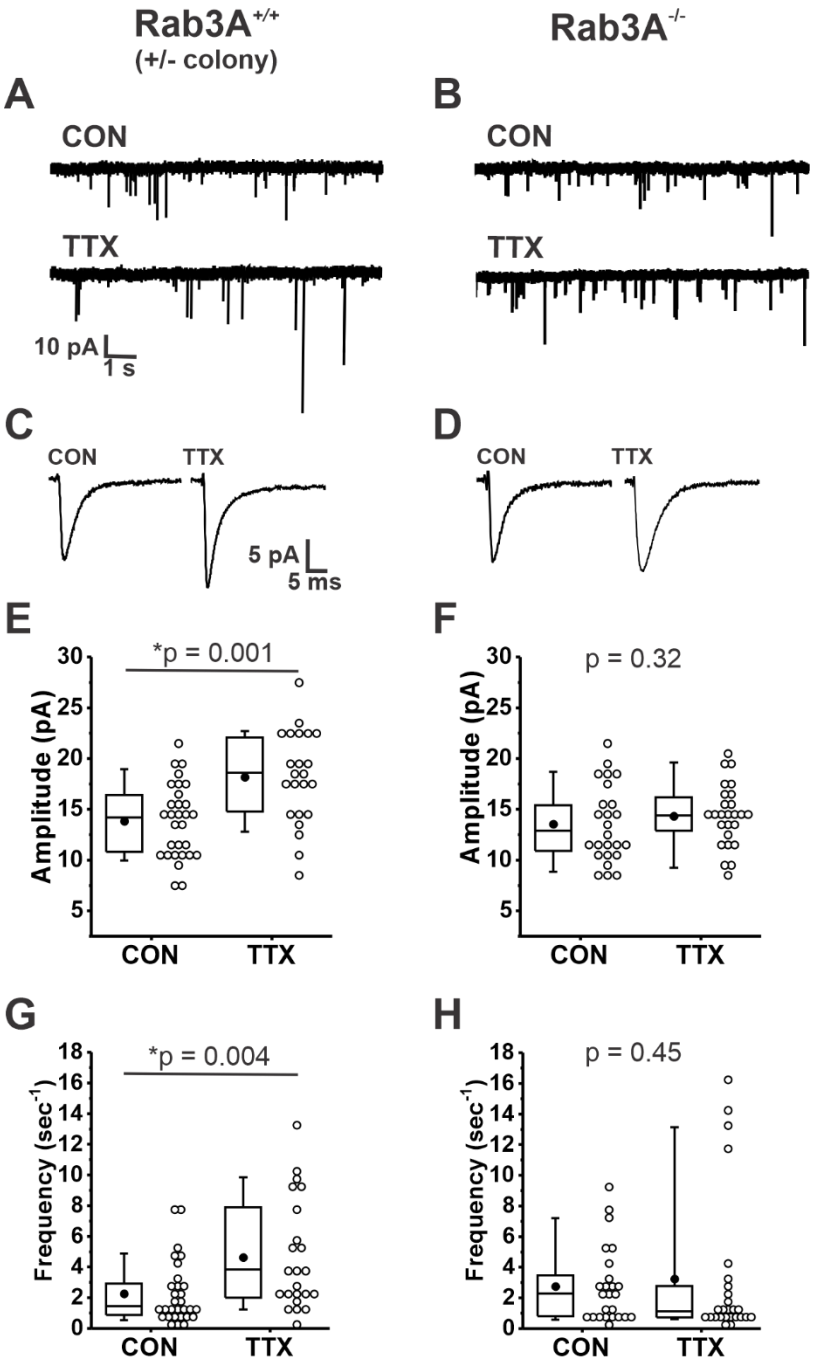

Figure 1. Loss of Rab3A disrupted the TTX-induced increase in amplitudes of mEPSCs recorded in cultured mouse cortical neurons; the increase in frequency was more variable but also appears to be reduced.

(A) Ten second example traces recorded at -60 mV in pyramidal cortical neurons from an untreated ("CON") and TTX-treated ("TTX") neuron in cultures prepared from Rab3A$^{+/+}$ mice from the Rab3A$^{+/-}$ colony. (B) Ten second example traces recorded at -60 mV in pyramidal cortical neurons from an untreated ("CON") and TTX-treated ("TTX") neuron in cultures

prepared from Rab3A$^{-/-}$ mice. (C & D) Average traces for the recordings shown in A and B, respectively. (E) Box plots for average mEPSC amplitudes from untreated cells and TTX-treated cells in cultures prepared from Rab3A$^{+/+}$ mice (Rab3A$^{+/-}$ colony; CON, N = 30 cells, 13.9 ± 0.7 pA; TTX, N = 23 cells, 18.2 ± 0.9 pA; from 11 cultures). (F) Box plots for average mEPSC amplitudes from untreated cells and TTX-treated cells in cultures prepared from Rab3A$^{-/-}$ mice (CON, N = 25 cells, 13.6 ± 0.7 pA; TTX, N = 26 cells, 14.3 ± 0.6 pA); from 11 cultures. (G) Box plots for average mEPSC frequency for same Rab3A$^{+/+}$ cells as in (E) (CON, 2.26 ± 0.37 sec^{-1}; TTX, 4.62 ± 0.74 sec^{-1}). (H) Box plots for average mEPSC frequency for same Rab3A$^{-/-}$cells as in (F) (CON, 2.74 ± 0.49 sec^{-1}; TTX, 3.23 ± 0.93 sec^{-1}). Box plot parameters: box ends, 25th and 75th percentiles; whiskers, 10th and 90th percentiles; open circles represent means from individual cells, bin size 1 pA, 0.5 sec^{-1}; line, median; dot, mean. p values (shown on the graphs) are from Kruskal-Wallis test. For all p-values, * with underline indicates significance with $p < 0.05$.

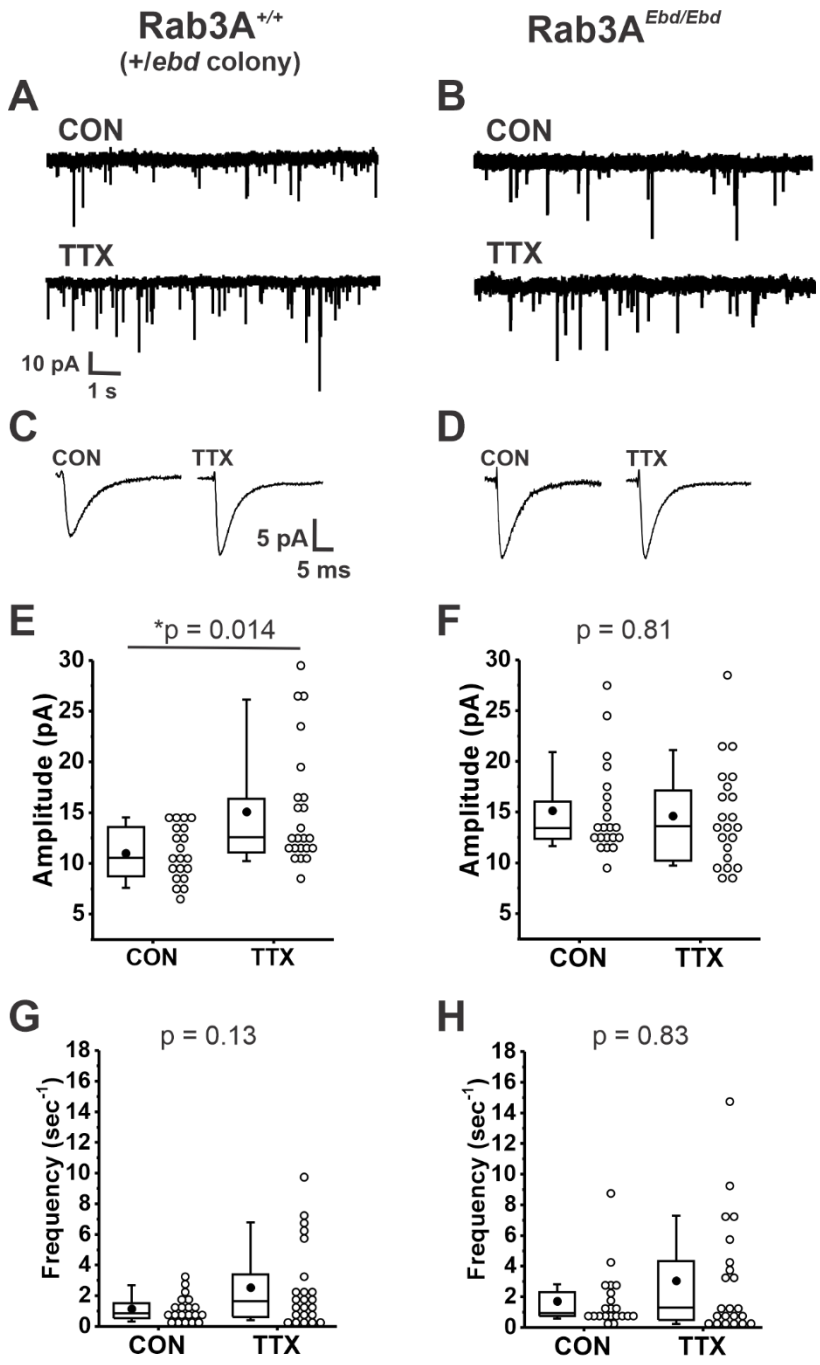

Figure 2. Normally functioning Rab3A was required for TTX-induced homeostatic plasticity of mEPSC amplitudes in cultured mouse cortical neurons.

(A) Ten second example traces recorded at -60 mV in pyramidal cortical neurons from an untreated ("CON") and TTX-treated ("TTX") neuron in cultures prepared from Rab3A$^{+/+}$ mice from the Rab3A$^{+/Ebd}$ colony. (B) Ten second example traces recorded at -60 mV in pyramidal cortical neurons from an untreated ("CON") and TTX-treated ("TTX") neuron in cultures

prepared from Rab3A$^{Ebd/Ebd}$ mice. (C & D) Average traces for the recordings shown in A and B, respectively. (E) Box plots for average mEPSC amplitudes from untreated cells and TTX-treated cells from cultures prepared from Rab3A$^{+/+}$ mice (Rab3A$^{+/Ebd}$ colony; CON, N = 20 cells, 11.0 ± 0.6 pA; TTX, N = 23 cells, 15.1 ± 1.2 pA; from 6 cultures). (F) Box plots for average mEPSC amplitudes from untreated cells and TTX-treated cells from cultures prepared from Rab3A$^{Ebd/Ebd}$ mice (CON, N = 21 cells, 15.1 ± 1.0 pA; TTX, N = 22 cells, 14.6 ± 1.1 pA; from 7 cultures.) (G) Box plots for average mEPSC frequency for same Rab3A$^{+/+}$ cells as in (E) (CON, 1.15 ± 0.19 sec^{-1}; TTX, 2.54 ± 0.55 sec^{-1}). (H) Box plots for average mEPSC frequency for same Rab3A$^{Ebd/Ebd}$ cells as in (F) (CON, 1.71 ± 0.41 sec^{-1}; TTX, 3.05 ± 0.80 sec^{-1}). Box plot parameters: box ends, 25th and 75th percentiles; whiskers, 10th and 90th percentiles; open circles represent means from individual cells; bin size 1 pA, 0.5 sec^{-1}; line, median; dot, mean. p values (shown on the graphs) are from Kruskal-Wallis test. For all p-values, * with underline indicates significance with $p < 0.05$.

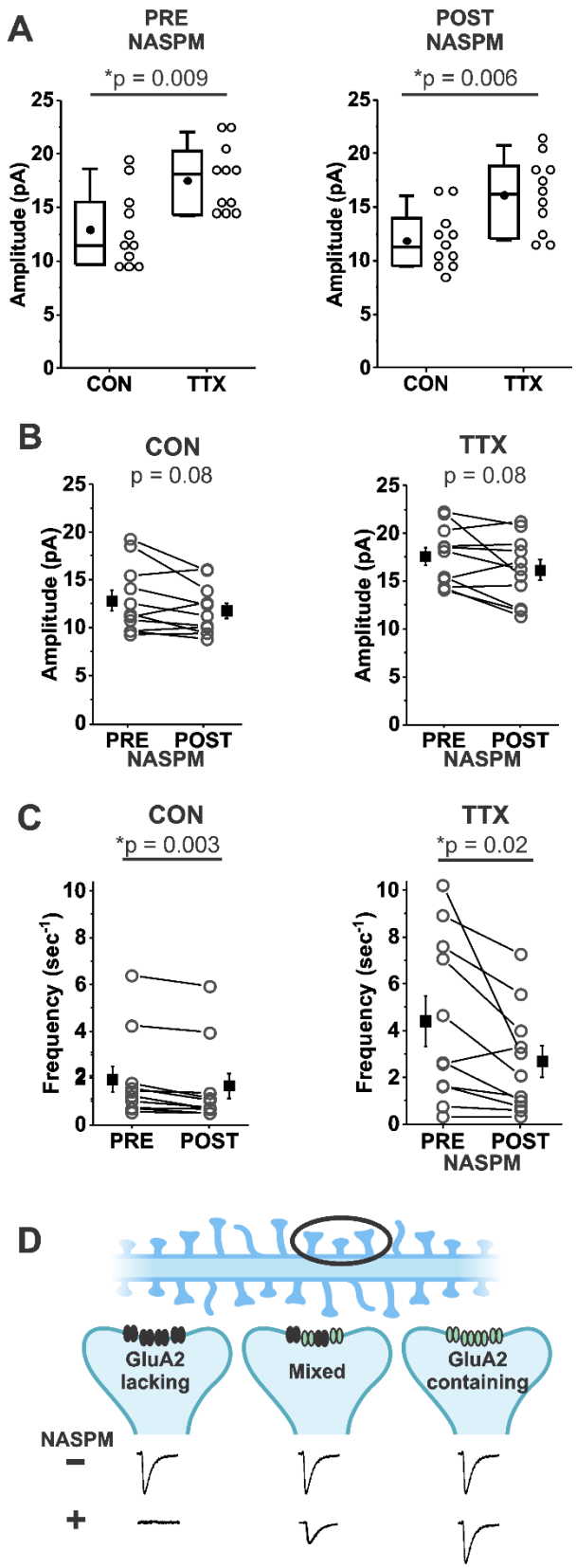
A
PRE NASPM
*p = 0.009
POST NASPM
*p = 0.006
Amplitude (pA)
CON
TTX
B
CON
p = 0.08
TTX
p = 0.08
PRE
POST
NASPM
C
CON
*p = 0.003
TTX
*p = 0.02
Frequency (sec-1)
D
GluA2 lacking
Mixed
GluA2 containing
NASPM
−
+

Figure 3

Figure 3. Homeostatic plasticity of mEPSC amplitudes in mouse cortical cultures treated with TTX for 48 hr was unchanged by acute inhibition of Ca^{2+} permeable AMPA receptors by NASPM (20 μm).

(A) Box plot comparison of the TTX effect on mEPSC amplitudes in the same pyramidal neurons before and after application of 20 μM NASPM. (N = 11 cells from 3 cultures; Pre-NASPM, CON: 12.9 ± 1.1 pA; TTX: 17.5 ± 0.9 pA; post-NASPM, CON: 11.9 ± 0.8 pA; TTX: 16.1 ± 1.0 pA). (B) Line series plot of mEPSC amplitudes before and after acute perfusion with 20 μM NASPM for untreated and TTX-treated pyramidal neurons; same cells as in (A); CON, pre-NASPM: 12.9 ± 1.1 pA; post-NASPM: 11.9 ± 0.8 pA; TTX, pre-NASPM: 17.5 ± 0.9 pA; post-NASPM: 16.1 ± 0.1 pA. (C) Line series plot of mEPSC frequency before and after acute perfusion with 20 μM NASPM for untreated and TTX-treated pyramidal neurons; same cells as in (A); CON, pre-NAPSM: 1.84 ± 0.55 sec^{-1}; post-NASPM; 1.56 ± 0.53 sec^{-1}; TTX, pre-NASPM: 4.40 ± 1.06 sec^{-1}; post-NASPM, 2.68 ± 0.68 sec^{-1}. (D) A proposed mechanism for why NASPM had a robust effect on frequency without greatly affecting amplitude. A dendrite with spines (Top) is expanded on three postsynaptic sites (Middle) to show possible types of AMPA receptor distributions: Left, at a site comprised only of Ca^{2+}-permeable AMPA receptors (NASPM-sensitive, GluA2-lacking receptors (black)), NASPM would completely inhibit the mEPSC, causing a decrease in frequency to be measured in the overall population; Right, at a site comprised only of Ca^{2+}-impermeable AMPA receptors (NASPM-insensitive, GluA2-containing receptors (green)), NASPM would have no effect on mEPSC amplitude; Middle, at a site comprised of a mix of Ca^{2+}-permeable and Ca^{2+}-impermeable AMPA receptors, NASPM would partially inhibit the mEPSC. Diagram produced in BioRender.com (2024). Box plot parameters: box ends, 25th and 75th percentiles; whiskers, 10th and 90th percentiles; open circles represent means from individual cells; bin size 1 pA; line, median; dot, mean. p values (shown on the graphs) are from Kruskal-Wallis test. Line series plot p values are from student's paired t test. For all p-values, * with underline indicates significance with $p < 0.05$.

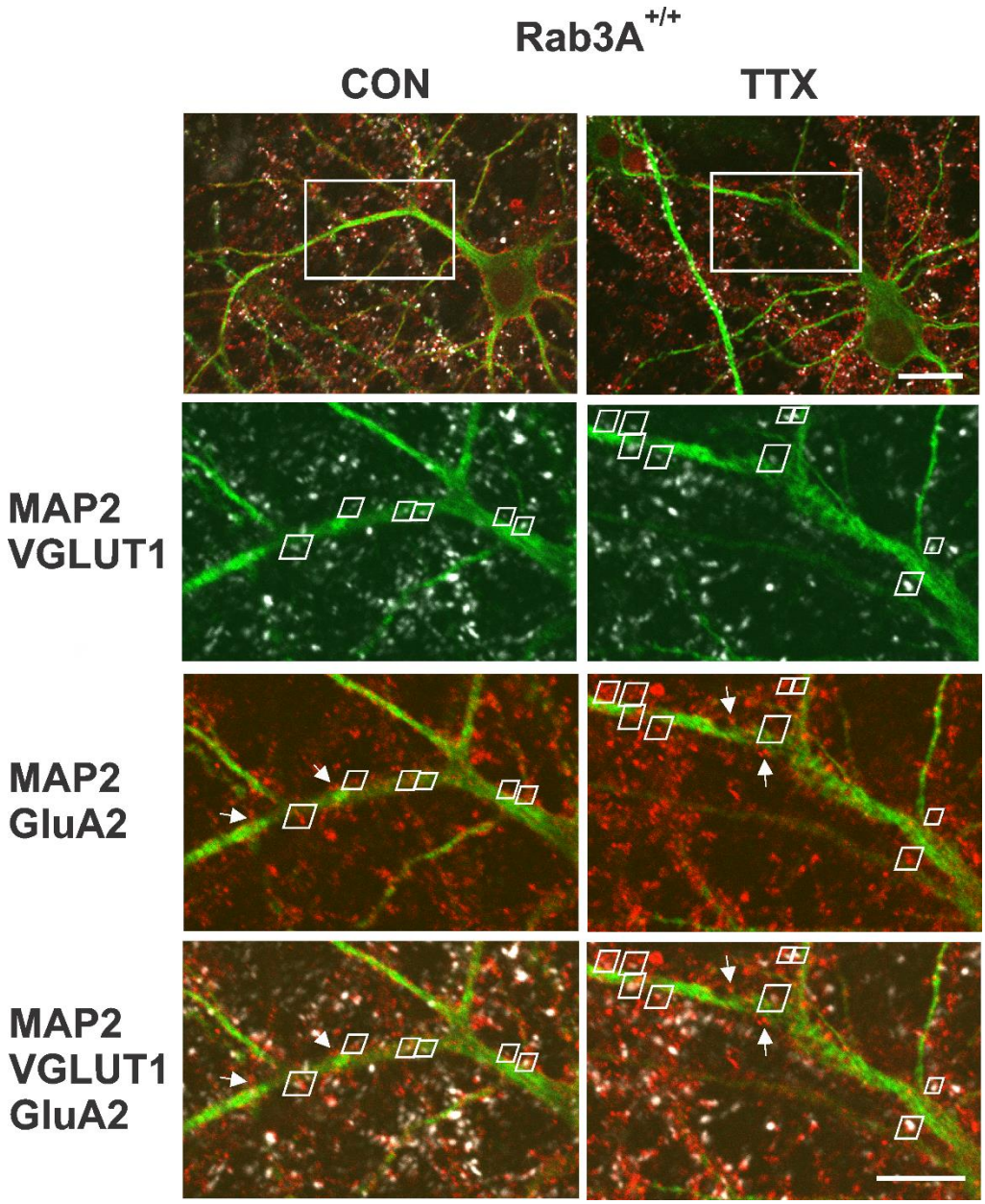

Figure 4. Identification of synaptic GluA2 receptor immunofluorescence on primary dendrites of pyramidal neurons in high density mouse cortical co-cultures prepared from Rab3A$^{+/+}$ mice.

(Top) Non-zoomed single confocal sections collected with a 60X oil immersion objective of recognizably pyramidal-shaped neurons, presumed to be excitatory neurons, selected for synaptic GluA2 analysis. A neuron was selected from an untreated coverslip (CON, Left) and a TTX-treated coverslip (TTX, Right) from the same culture prepared from Rab3A$^{+/+}$ animals (= Rab3A$^{+/+}$ Culture #2 in Figure 5). The white rectangular boxes indicate 5X zoomed areas shown in the images below. Note that the depth of the single confocal section of the non-zoomed neuron image is not at the same depth as the confocal section in zoomed dendritic image, so

some features are not visible in both images. Scale bar, 20 μm. (Bottom) 5X zoom single confocal sections selected for demonstration purposes because they had an unusually high number of identified synaptic pairs along the primary dendrite contained within a single confocal section. Synaptic pairs, highlighted with white trapezoids, were identified based on close proximity of GluA2 (red) and VGLUT1 (white) immunofluorescence, apposed to the MAP2 immunofluorescent primary dendrite (green). Some apparent synaptic pairs are not highlighted with a white trapezoid because there was a different confocal section in which the two immunofluorescent sites were maximally bright. There were GluA2 positive clusters located on the primary dendrites that were not apposed to VGLUT1-positive terminals (4 of these non-synaptic GluA2 clusters are highlighted with white arrows in the MAP2-GluA2 and MAP2-GluA2-VGLUT1 panels). Scale bar, 10 μm.

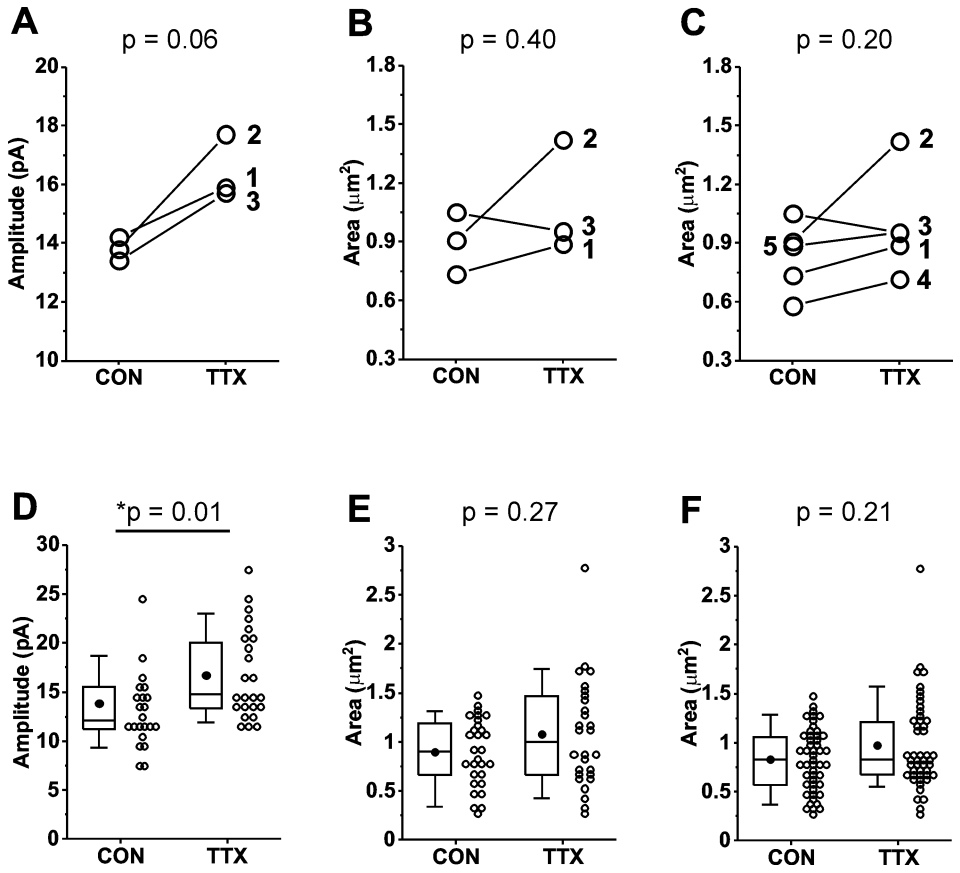

Figure 5. Comparison of mEPSC amplitudes and GluA2 receptor cluster areas in matched and unmatched mouse cortical cultures prepared from Rab3A$^{+/+}$ mice and treated with TTX for 48 hr.

(A) Culture averages of mEPSC amplitudes for untreated (CON) and TTX-treated coverslips (TTX) in each of 3 Rab3A$^{+/+}$ mouse cortical co-cultures. Culture #1, CON, N = 6, 14.2 $\pm$ 2.2 pA; TTX, N = 6, 15.9 $\pm$ 1.9 pA; Culture #2, CON, N = 7, 13.8 $\pm$ 2.4 pA; TTX, N = 8, 17.7 $\pm$ 1.8 pA; Culture #3, CON, N = 10, 13.4 $\pm$ 0.8 pA; TTX, N = 9, 15.7 $\pm$ 1.0 pA. (B) Culture averages of GluA2 receptor cluster size in the same 3 cultures as shown in (A). Culture #1, CON, N = 10, 0.73 $\pm$ 0.09 μm^2; TTX, N = 9, 0.89 $\pm$ 0.09 μm^2; Culture #2, CON, N = 9, 0.91 $\pm$ 0.12 μm^2; TTX, N = 9, 1.42 $\pm$ 0.24 μm^2; Culture #3, CON, N = 10, 1.05 $\pm$ 0.11 μm^2; TTX, N = 9, 0.95 $\pm$ 0.15 μm^2. (C) Two additional culture averages are included that did not have corresponding mEPSC recordings. Culture #4, CON, N = 10, 0.58 $\pm$ 0.07 μm^2: TTX, N = 10, 0.71 $\pm$ 0.04 μm^2; Culture 5, CON, N =10, 0.89 $\pm$ 0.05 μm^2; TTX, N = 10, 0.95 $\pm$ 0.08 μm^2. (D) Box plots of cell mean mEPSC amplitudes pooled from same 3 cultures as shown in (A). CON, N = 23 cells, 13.7 $\pm$ 0.9 pA; TTX, N = 24 cells, 16.4 $\pm$ 0.9 pA. (E) Box plots of dendrite mean GluA2 receptor cluster size pooled from same 3 cultures as shown in (A) and (B). CON, N = 29 dendrites, 0.90 $\pm$ 0.06 μm^2; TTX, N = 28 dendrites, 1.08 $\pm$ 0.10 μm^2. (F) Box plots of dendrite mean GluA2 receptor cluster size pooled from the same 5

cultures shown in (C). CON, N = 49 dendrites, 0.83 $\pm$ 0.04 μm^2; TTX, N = 48 dendrites, 0.98 $\pm$ 0.07 μm^2. Line series, Student's paired T test; box plots, Kruskal-Wallis test. Box plot parameters: box ends, 25th and 75th percentiles; whiskers, 10 and 90 percentiles; open circles indicate means of individual cells/dendrites; bin size 1 pA, 0.5 μm^2; line, median; dot, mean. For all p-values, * with underline indicates significance with $p < 0.05$.

.

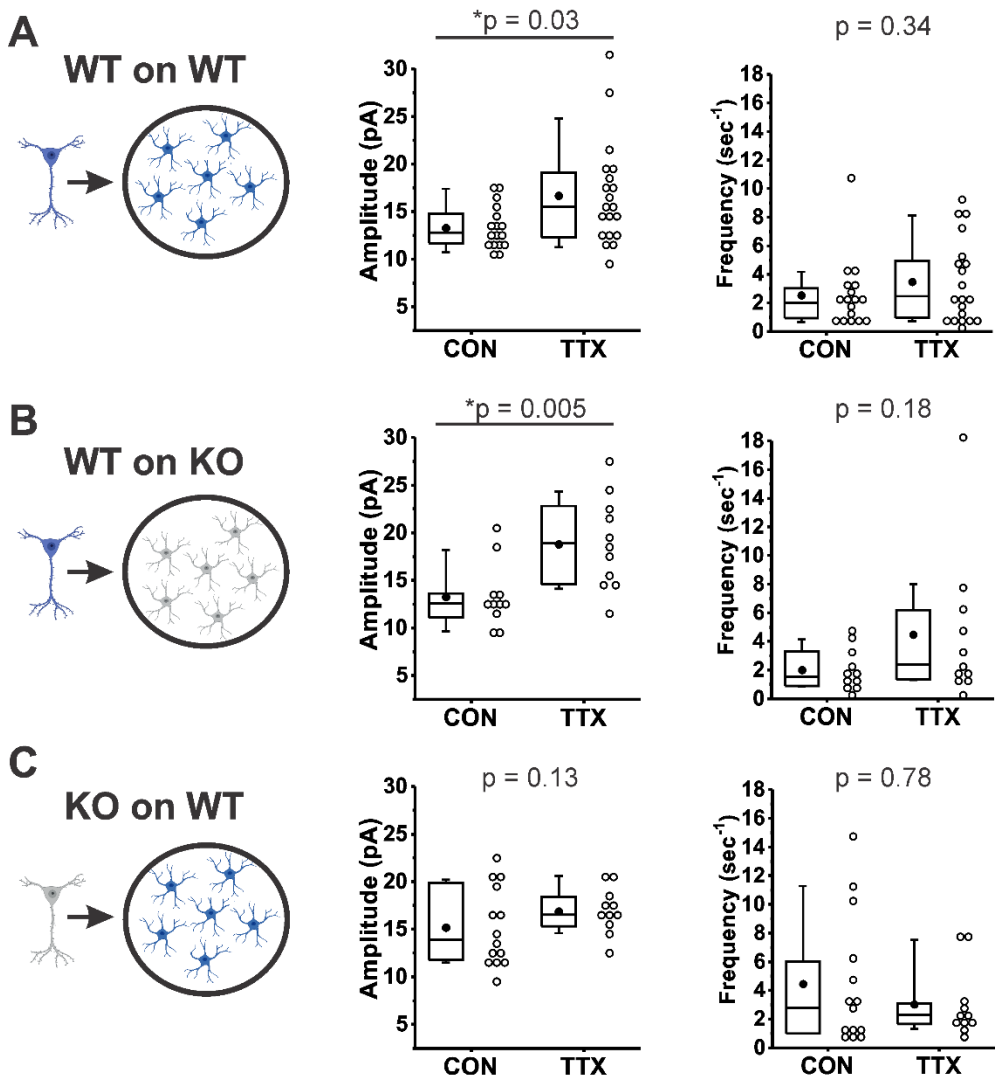

Figure 6. Rab3A in neurons, not astrocytes, was required for full TTX-induced homeostatic plasticity.

(A)-(C), mEPSC amplitude (Middle) and frequency (Right) data from dissociated cortical neurons plated on an astrocyte feeder layer, each prepared separately from the type of mice depicted in the schema (Left): (A) Neurons from Rab3A$^{+/+}$ mice plated on astrocytes from Rab3A$^{+/+}$ mice. Box plots for mEPSC amplitudes (CON, N = 17 cells, 13.3 ± 0.5 pA; TTX, N = 20 cells, 16.7 ± 1.2 pA) and mEPSC frequency in the same recordings (mean, CON, 2.54 ± 0.57 sec^{-1}; TTX, 3.48 ± 0.64 sec^{-1}); from 4 cultures. (B) Neurons from Rab3A$^{+/+}$ mice plated on astrocytes from Rab3A$^{-/-}$ mice. Box plots for average mEPSC amplitude (CON, N = 11 cells, 13.3 ± 1.0 pA; TTX, N = 11 cells,

18.8 ± 1.4 pA) and average mEPSC frequency in the same recordings (CON, 2.01 ± 0.41 sec^{-1}; TTX, 4.47 ± 1.53 sec^{-1}); from 2 cultures. (C) Neurons from $Rab3A^{-/-}$ neurons plated on astrocytes from $Rab3A^{+/+}$ mice. Box plots for average mEPSC amplitude (CON, N = 14 cells, 15.2 ± 1.1 pA; TTX, N = 11 cells, 16.9 ± 0.7 pA) and mEPSC frequency in the same recordings (CON, 4.47 ± 1.21 sec^{-1}; TTX, 3.02 ± 0.70 sec^{-1}); from 3 cultures. Box plot parameters: box ends, 25th and 75th percentiles; whiskers, 10th and 90th percentiles; open circles represent means from individual cells; line, median; dot, mean. p values (shown on the graphs) are from Kruskal-Wallis test. p-values denoted with * and underline indicates significance of $p < 0.05$.

890

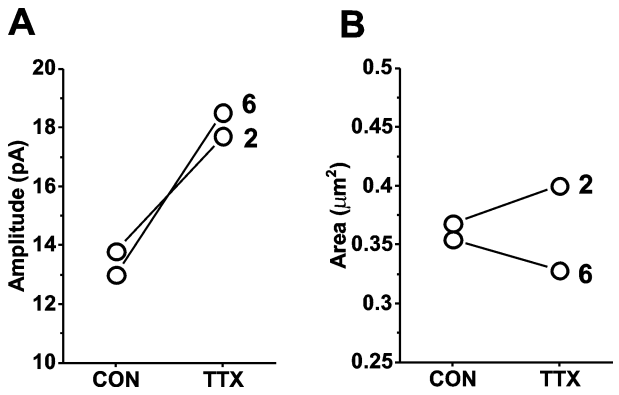

Supplemental Figure 1. Comparison of mEPSC amplitudes and GluA1 receptor cluster areas in matched mouse cortical cultures prepared from Rab3A$^{+/+}$ mice and treated with TTX for 48 hr.

(A) Culture averages of mEPSC amplitudes for untreated (CON) and TTX-treated coverslips (TTX) in each of 2 Rab3A$^{+/+}$ mouse cortical co-cultures. Culture #2, CON, N = 7, 13.8 $\pm$ 2.4 pA; TTX, N = 8, 17.7 $\pm$ 1.8 pA (+28.3%); Culture #6, CON, N = 6, 13.0 $\pm$ 1.5 pA; TTX, N = 6, 18.5 $\pm$ 2.0 pA (+42.3%). (B) Culture averages of GluA1 receptor cluster size in the same 2 cultures as shown in (A). Culture #2, CON, N = 10, 0.37 $\pm$ 0.04 μm^2; TTX, N = 10, 0.40 $\pm$ 0.06 μm^2 (+8.1%) Culture #6, CON, N = 10, 0.35 $\pm$ 0.05 μm^2; TTX, N = 10, 0.33 $\pm$ 0.04 μm^2 (-5.7%) "Culture #2" is the same Culture #2 depicted in Figure 5, different coverslips were processed for GluA1 immunofluorescence labeling. GluA1 receptor cluster intensity did not increase in Culture #2 (CON, 364 vs. TTX, 357) or Culture #6 (CON, 357 vs. TTX, 363). Live cultures were exposed to GluA1 antibody against the extracellular domain (ABN241, purchased from EMD Millipore, now available from Millipore Sigma) before being fixed and processed with secondary antibodies.

Table 1. Comparison of mEPSC amplitude and GluA2 receptor cluster characteristics in mouse cortical cultures prepared from Rab3A$^{+/+}$ mice, and Rab3A$^{-/-}$ mice.

	Rab3A$^{+/+}$				**Rab3A$^{-/-}$**			
Quantity	**CON Mean, SE**	**TTX Mean, SE (N, cultures)**	**% change**	**p value**	**CON Mean, SE (N, cultures)**	**TTX Mean, SE (N, cultures)**	**% change**	**p value**
mEPSC amplitude	13.7 ± 0.9 pA (23 cells, 3 cultures)	16.4 ± 0.9 pA (24 cells, 3 cultures)	+19.7	*p = 0.02	14.9 ± 0.8 pA (21 cells, 3 cultures)	13.5 ± 0.9 pA (21 cells, 3 cultures)	-9.4	p = 0.18
GluA2 cluster size	0.83 ± 0.04 μm^2 (49 cells, 5 cultures)	0.98 ± 0.07 μm^2 (48 cells, 5 cultures)	+18.1	p = 0.21	0.93 ± 0.05 μm^2 (30 cells, 3 cultures)	0.91 ± 0.05 μm^2 (29 cells, 3 cultures)	-2.2	p = 0.75
GluA2 cluster intensity	733 ± 14 a.u. (49 cells, 5 cultures)	738 ± 13 a.u. (48 cells, 5 cultures)	+0.7	p = 0.69	766 ± 12 a.u. (30 cells, 3 cultures)	776 ± 15 a.u. (29 cells, 3 cultures)	+1.3	p = 0.46
GluA2 cluster integral	311021 ± 19282 a.u. (49 cells, 5 cultures)	365366 ± 27080 a.u. (48 cells, 5 cultures)	+17.4	p = 0.22	369436 ± 23439 a.u. (30 cells, 3 cultures)	364237 ± 25833 a.u. (29 cells, 3 cultures)	-0.8	p = 0.86

Table 2. Comparison of mEPSC amplitude and VGLUT1 positive presynaptic site characteristics in mouse cortical cultures prepared from Rab3A$^{+/+}$ and Rab3A$^{-/-}$ mice. mEPSC data are identical to that in Table 1, reproduced here for comparison purposes.

	Rab3A$^{+/+}$				**Rab3A$^{-/-}$**			
Quantity	**CON Mean, SE**	**TTX Mean, SE**	**% change**	**p value**	**CON Mean, SE**	**TTX Mean, SE**	**% change**	**p value**
mEPSC amplitude	13.7 ± 0.9 pA (23 cells, 3 cultures)	16.4 ± 0.9 pA (24 cells, 3 cultures)	+19.7	*p = 0.02	14.9 ± 0.8 pA (21 cells, 3 cultures)	13.5 ± 0.9 pA (21 cells, 3 cultures)	-9.4	p = 0.18
VGLUT1 site size	1.17 ± 0.08 μm^2 (29 cells, 3 cultures)	1.07 ± 0.06 μm^2 (24 cells, 3 cultures)	-7.7	p = 0.97	0.89 ± 0.03 μm^2 (30 cells, 3 cultures)	0.95 ± 0.04 μm^2 (29 cells, 3 cultures)	+6.7	p = 0.55
VGLUT1 site intensity	699 ± 39 a.u. (29 cells, 3 cultures)	639 ± 31 a.u. (28 cells, 3 cultures)	-8.6	p = 0.28	554 ± 13 a.u. (30 cells, 3 cultures)	570 ± 19 a.u. (29 cells, 3 cultures)	+2.9	p = 0.18
VGLUT1 site integral	430787 ± 36818 a.u. (29 cells, 3 cultures)	351653 ± 21689 a.u. (28 cells, 3 cultures)	-18.4	p = 0.13	257159 ± 18265 a.u. (30 cells, 3 cultures)	289857 ± 18521 a.u. (29 cells, 3 cultures)	+12.7	p = 0.21